

# Removal of toxic steroidal glycoalkaloids and bitterness in tomato is controlled by a complex epigenetic and genetic network

Feng Bai<sup>1</sup>, Mengbo Wu<sup>1</sup>, Wei Huang<sup>2</sup>, Weijie Xu<sup>1</sup>, Yikui Wang<sup>3</sup>, Yang Zhang<sup>1</sup>, Zhenhui Zhong<sup>1</sup>, Yiguo Hong<sup>4,5</sup>, Julien Pirrello<sup>6</sup>, Mondher Bouzayen<sup>1,6</sup>, Mingchun Liu<sup>1\*</sup>

The steroidal glycoalkaloids (SGAs) produced in *Solanaceae* crops, including tomato, are antinutritional because of their cellular toxicity and resultant bitter taste to humans. To make fruits palatable, SGA profiles shift from bitter and toxic  $\alpha$ -tomatine to nonbitter and nontoxic esculeoside A during the ripening process. However, the mechanisms regulating this conversion remain unclear. In this study, we showed that removal of toxic and bitter SGAs is under the control of DNA demethylation, ethylene, and key transcription factors by forming a feedback loop that governs the expression of key *GLYCOALKALOID METABOLISM (GAME)* genes during ripening. Moreover, the ethylene-inducible transcription factors NON-RIPENING, RIPENING INHIBITOR, and FRUITFULL1 coordinately regulate the expression of *GAME31*, *GAME40*, *GAME5*, and the glycoalkaloid transporter gene *GORKY*, whereas jasmonic acid-induced *MYC2* modulates the transcription of *GAME36*. Furthermore, DNA demethylation mediated by the *DEMENTER-LIKE 2* drives SGA detoxification during tomato domestication.

## INTRODUCTION

Steroidal glycoalkaloids (SGAs) are well-known metabolites produced by *Solanaceae* species; these defense-related compounds affect pathogen infection and mammalian feeding (1–3). Although SGAs are important for crop resistance against pathogens and herbivores, they are also antinutritional substances because they are toxic and have bitter or unpleasant tastes (4, 5). In *Solanaceae* such as tomato (*Solanum lycopersicum*), the conversion from toxic, bitter compounds to nontoxic and nonbitter compounds during ripening may have been evolutionarily important as edible and palatable fruits can be beneficial for seed dispersal by animals.

The SGA metabolic pathway starts with cholesterol; in tomato, cholesterol is converted to  $\alpha$ -tomatine, the major SGA in green tissues, including leaves, stems, and fruit (1). To prevent self-toxicity,  $\alpha$ -tomatine is stored in the vacuole; during ripening, the nitrate/peptide family transporter *GORKY* exports  $\alpha$ -tomatine from the vacuole to the cytosol, where it is converted into esculeoside A (4). Thus, as fruits ripen, their SGA profiles shift from bitter and toxic  $\alpha$ -tomatine to nonbitter and nontoxic esculeoside A. This shift involves a series of enzymatic hydroxylation, acetylation, and glycosylation steps executed by *GLYCOALKALOID METABOLISM (GAME)* proteins (1, 2, 6–8). *GAME31*, *GAME36*, *GAME40*, and *GAME5* all encode enzymes responsible for steps in the conversion from  $\alpha$ -tomatine to esculeoside A during fruit ripening (6, 9–11). Although the biochemical pathways of  $\alpha$ -tomatine biosynthesis and metabolism have been well studied in tomato (8, 12, 13), the regulatory network controlling SGA metabolism during fruit ripening remains largely unknown.

Copyright © 2025 The Authors, some rights reserved; exclusive licensee American Association for the Advancement of Science. No claim to original U.S.

Government Works. Distributed under a Creative Commons Attribution NonCommercial License 4.0 (CC BY-NC).

In plants, DNA methylation occurs predominantly at cytosine bases (5-mC) in the asymmetric CHH context and in the symmetric CG and CHG contexts (where H = A, C, or T) (14, 15). DNA methylation is dynamic and can be lost through failure to maintain methylation after replication or through active removal (DNA demethylation) (16, 17). Tomato has four annotated 5-mC DNA glycosylase/DNA demethylase genes, among which the expression of *DEMENTER-LIKE 2 (DML2)* is strongly induced during fruit ripening (18, 19). Overall DNA methylation levels decrease during fruit ripening; application of the DNA methylation inhibitor 5-azacytidine to plants changes the genome-wide DNA methylation landscape and accelerates ripening in tomato (20). Moreover, knockdown or knockout of *DML2* in tomato inhibits fruit ripening (18, 21), indicating that active DNA demethylation plays critical role in regulating fruit ripening. Notably, although the conversion from  $\alpha$ -tomatine to esculeoside A occurs during ripening, whether DNA methylation is involved in this step remains unknown.

The phytohormone ethylene, key transcription factors (TFs), and epigenetic modifications are essential for the regulation of climacteric fruit ripening (22, 23). In tomato, a model climacteric fruit species, ethylene is the main trigger of fruit ripening (22–24). In addition, TFs such as RIPENING INHIBITOR (RIN), NON-RIPENING (NOR), COLORLESS NONRIPENING (CNR), TOMATO AGAMOUS-LIKE1 (TAGL1), and FRUITFULL 1 (FUL1) also play vital roles in regulating tomato fruit ripening (24–30). SGA metabolism is affected in ripening-defective mutants such as *rin* and *nor*; in *rin*, this may involve effects on the expression of *GAME* genes such as *GAME1* (2, 29). These studies have suggested a possible link between the abovementioned ripening-related TF and SGA metabolism during fruit ripening. Moreover, the *RIN* and *NOR* loci are hypermethylated and their expression is down-regulated during ripening in lines with RNA interference-induced *DML2* knockdown and in lines carrying a loss-of-function mutation of *DML2* (21), suggesting a direct link between ripening-related TF and DNA methylation during ripening. Nevertheless, the exact relationship between these ripening-related TF and DNA methylation and its effect in controlling the conversion of SGAs during ripening is still unknown.

In this study, using whole-genome bisulfite sequencing (WGBS) data and a knockout mutant of *DML2*, we revealed that DNA

<sup>1</sup>Key Laboratory of Bio-Resource and Eco-Environment of Ministry of Education, College of Life Sciences, Sichuan University, Chengdu 610065, China. <sup>2</sup>State Key Laboratory of Agricultural Genomics, Key Laboratory of Genomics, Ministry of Agriculture, BGI Research, Shenzhen, Guang Dong 518083, China. <sup>3</sup>Guangxi Academy of Agricultural Sciences, Nanning 530007, Guangxi, China. <sup>4</sup>School of Life Sciences, University of Warwick, Warwick CV4 7AL, UK. <sup>5</sup>State Key Laboratory of North China Crop Improvement and Regulation and College of Horticulture, Hebei Agricultural University, Baoding 071000, China. <sup>6</sup>Laboratoire de Recherche en Sciences Végétales-Génomique et Biotechnologie des Fruits-UMR5546, Université de Toulouse, CNRS, UPS, Toulouse-INP, Toulouse, France.

\*Corresponding author. Email: mcliu@scu.edu.cn

demethylation has a critical role in the conversion of SGAs during ripening. Moreover, we demonstrated that the TFs NOR, RIN, FUL1, and MYC2 regulate the expression of *GAME* genes responsible for SGA metabolism during ripening, forming a regulatory network that controls the reduction in SGA toxicity and bitterness during fruit ripening. In addition, we found that *DML2*-mediated DNA demethylation drives the removal of toxic SGA during tomato domestication. This study not only provides fresh insights into the regulatory mechanism of SGA conversion during fruit ripening but also sheds light on options for breeding tomato to balance resistance and quality by modulating SGA metabolism.

## RESULTS

### DNA demethylation is involved in SGA metabolism during fruit ripening

As tomato fruit ripening progresses, SGA profiles shift from  $\alpha$ -tomatine to esculeoside A via four key enzymes encoded by *GAME31*, *GAME36*, *GAME40*, and *GAME5* (Fig. 1, A and B, and fig. S1A). Three of these four *GAME* genes (*GAME31*, *GAME40*, and *GAME5*) displayed increased expression along with fruit ripening, whereas *GAME36* was expressed evenly across all fruit developmental and ripening stages (Fig. 1C). Because genome-wide DNA methylation levels decrease during tomato fruit ripening, we wondered whether DNA methylation might be involved in SGA metabolism during ripening. Mining published DNA methylation datasets (20), we determined that DNA methylation levels at the promoters of the four *GAME* genes do not show significant changes at the green stages [17 days postanthesis (DPA) and 39 DPA] but significantly decrease when ripening is initiated (from 39 to 60 DPA) (Fig. 1D).

Because DNA methylation is also reported to regulate gene expression by affecting chromatin accessibility (31), we searched published databases (20) for a list of deoxyribonuclease (DNase) I hypersensitivity sites (DHS) to explore the relationship between DNA methylation and chromatin accessibility. The gradual decrease in DNA methylation observed over the *GAME31*, *GAME36*, *GAME40*, and *GAME5* promoters was correlated with increasing chromatin accessibility (fig. S1B). In addition, the expression of all four *GAME* genes gradually increased along with the increase in DNA demethylation (Fig. 1, C and D). These results suggest that DNA demethylation plays a critical role in SGA metabolism during tomato fruit ripening by modulating the expression of the four *GAME* genes participating in the conversion of  $\alpha$ -tomatine to esculeoside A.

### *DML2* controls SGA conversion during ripening by demethylating the chromatin of ripening-specific *GAME* genes

To explore the possible link between DNA demethylases and the control of SGA metabolism during fruit ripening, we performed a coexpression analysis using the transcriptome data for 4 DNA demethylase genes and 16 SGA metabolic genes. Among the four DNA demethylase genes, only *DML2* was coexpressed with the ripening-specific SGA metabolism genes *GAME31*, *GAME36*, *GAME40*, and *GAME5* (*r* value  $\geq 0.70$ ) (Fig. 1E). Notably, hyper-differentially methylated regions (hyper-DMRs) are present in the promoter regions of *GAME31*, *GAME36*, *GAME40*, and *GAME5* in the *dml2* mutant (a knockout line of *DML2*) (data S1). Furthermore, we analyzed the public WGBS database for tomato (21) to generate single-base resolution maps of DNA methylation and established that the

DNA methylation levels at the *GAME31*, *GAME36*, *GAME40*, and *GAME5* loci gradually decreases during fruit ripening from 25 to 46 DPA and to 60 DPA in wild type (WT) (Fig. 1F). Notably, in the *dml2* mutant, the DNA methylation levels along the promoter regions of the four *GAME* genes significantly increased during fruit ripening at 46 and 60 DPA compared to WT, with no difference between WT and *dml2* at the earlier stage of fruit development (25 DPA) (Fig. 1F). Moreover, the DNA hypermethylation of the *GAME31*, *GAME36*, *GAME40*, and *GAME5* loci occurred in all three sequence contexts in *dml2* mutant fruits (fig. S2). Consistent with the hypermethylation of their genomic regions, the expression levels of *GAME31*, *GAME40*, and *GAME5* were significantly down-regulated in the *dml2* mutant compared to WT at the red ripe stage (Fig. 1, G and H), whereas *GAME36*, whose expression pattern was distinct from that of the other three *GAME* genes (Fig. 1C), showed up-regulated expression in *dml2*. The expression levels of *GAME31*, *GAME40*, *GAME5*, and *GAME36* in WT and the *dml2-1* mutant agreed with the results of the reverse transcription quantitative polymerase chain reaction (RT-qPCR) analysis (fig. S3A). Overall, these data suggest that *DML2* contributes to DNA demethylation at the promoter regions of the ripening-specific *GAME* genes, thereby modulating the expression of these SGA metabolism genes.

To validate this hypothesis that DNA methylation is involved in the shift of the SGA profile during fruit ripening, we monitored the contents of SGAs in fruits by ultraperformance liquid chromatography–mass spectrometry (UPLC-MS). The contents of  $\alpha$ -tomatine, hydroxytomatine, acetoxytomatine, and acetoxy-hydroxytomatine increased in the *dml2* mutant at the red ripe stage compared to WT (Fig. 1I). However, the content of esculeoside A decreased by about 74% in the *dml2* mutant (Fig. 1I). These results confirm the critical role of *DML2* in SGA metabolism and support the notion that DNA demethylation controls the shift in SGA profile during tomato fruit ripening.

### Ethylene is the main plant hormone regulating the SGA pathway during ripening

Because a burst of ethylene occurs during ripening of climacteric fruits, and as the three *GAME* genes *GAME31*, *GAME40*, and *GAME5* exhibit a ripening-related expression pattern (Fig. 1A), we wished to investigate whether the expression of these ripening-related *GAME* genes is under ethylene control. To this end, we performed RT-qPCR to assess the transcript levels of the four *GAME* genes controlling SGA conversion during ripening using mature green (MG) fruits treated with ethylene and fruits at the breaker stage (Br) treated with 1-methylcyclopropene (1-MCP), a competitive inhibitor of ethylene. The relative expression levels of *GAME31*, *GAME40*, and *GAME5* were significantly increased in response to ethylene treatment and decreased in response to 1-MCP treatment (Fig. 2A). However, the expression of *GAME36* did not change significantly in response to ethylene treatment and increased in response to 1-MCP (Fig. 2A). The expression of *DML2* was also induced by ethylene but inhibited by 1-MCP treatment (Fig. 2A). We also examined the expression of the four *GAME* genes upon treatment with other plant hormones, including abscisic acid (ABA), gibberellin (GA), and jasmonic acid (JA). Treatment with methyl-jasmonate (MeJA) induced *GAME36* expression, whereas treatment with GA<sub>3</sub> repressed the expression of the three ripening-associated *GAME* genes; ABA treatment did not affect the expression levels of any of the four *GAME* genes (Fig. 2A). These results suggest that ethylene is a positive regulator of ripening-specific *GAME* genes, which will promote the conversion of  $\alpha$ -tomatine to esculeoside A during fruit ripening.

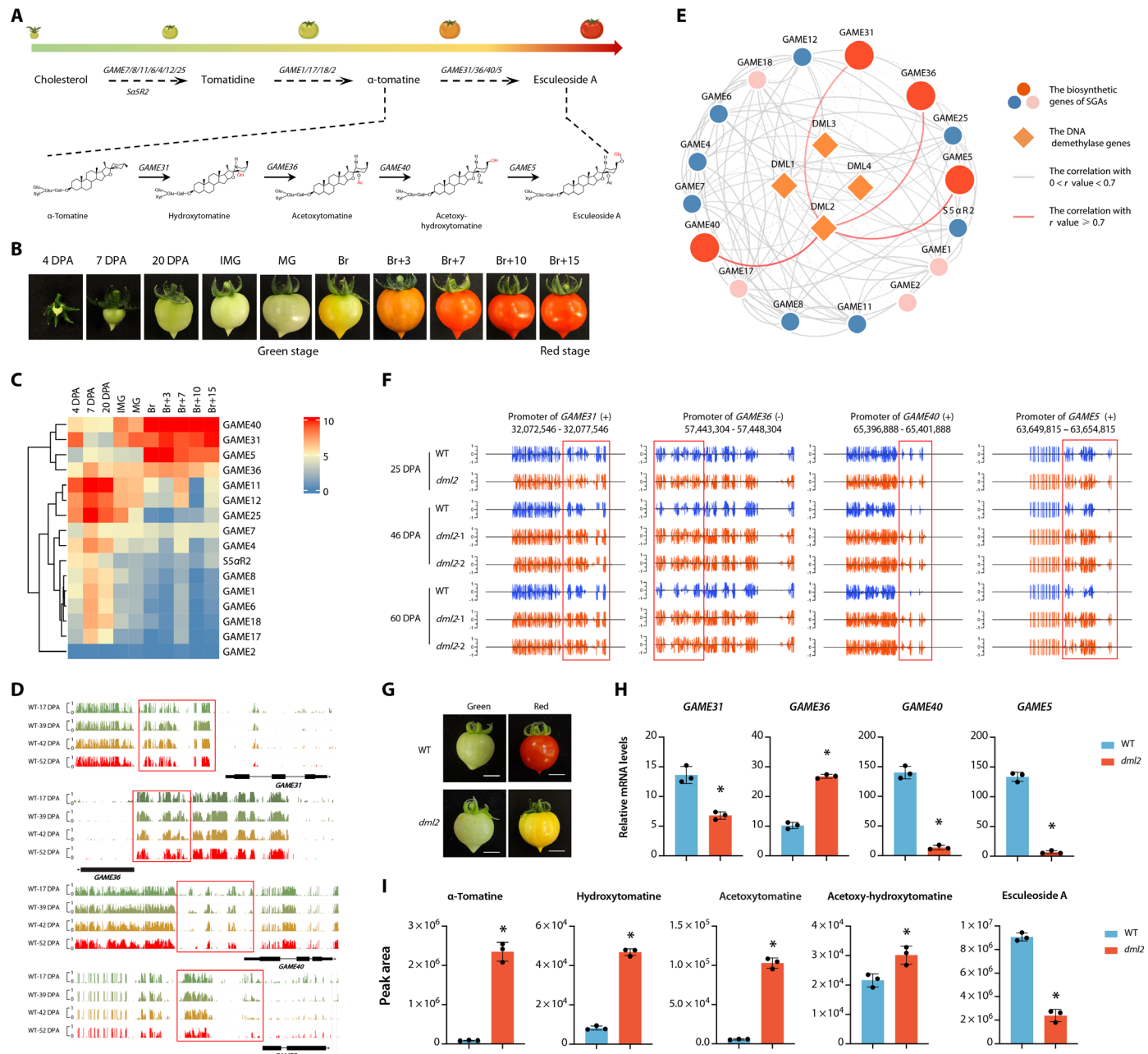


**Fig. 1. DNA methylation affects metabolic shifts in SGAs during tomato ripening.** (A) Biosynthetic pathway of esculeoside A during tomato fruit development and ripening. Specific activity displayed by these GAME enzymes is shown in red on the SGA structures. GAME, GLYCOALKALOID METABOLISM; Glu, glucose; Gal, galactose; Xyl, xylose; Ac, acetoxy. (B) Different stages of tomato growth and development. DPA, days postanthesis; IMG, immature green; MG, mature green; Br, breaker; Br+3, breaker plus 3 days. (C) Heatmap representation of the expression patterns of SGA biosynthesis genes and DNA demethylase genes. The normalized expression was extracted from the TomExpress database (<http://tomexpress.toulouse.inra.fr/>). (D) Screenshot of DNA methylation levels of four GAME genes and its promoters at different stages during ripening. Red boxed areas are DMRs. DMRs, differentially methylated regions. (E) Coexpression analysis of DNA demethylase genes and SGA biosynthesis genes using the transcriptome data. (F) Methylation levels at the promoters of four GAME genes in WT and *dml2* mutant fruits at 25-, 46-, and 60-DPA. Red boxed areas are hyper-DMRs. (G) Representative images of WT and *dml2* mutant fruits at green and red stages. Scale bars 10 mm. (H) Expression of GAME genes detected by RT-qPCR in WT and *dml2* fruits at the red stage. Data are presented as means  $\pm$  SD ( $n = 3$ ). \* $P < 0.05$  in two-sided  $t$  test. (I) SGA profiles of WT and *dml2* mutant fruits at the red stage. UPLC-MS was used for SGA profiling. Data are presented as means  $\pm$  SD ( $n = 3$ ). \* $P < 0.05$  in two-sided  $t$  test.

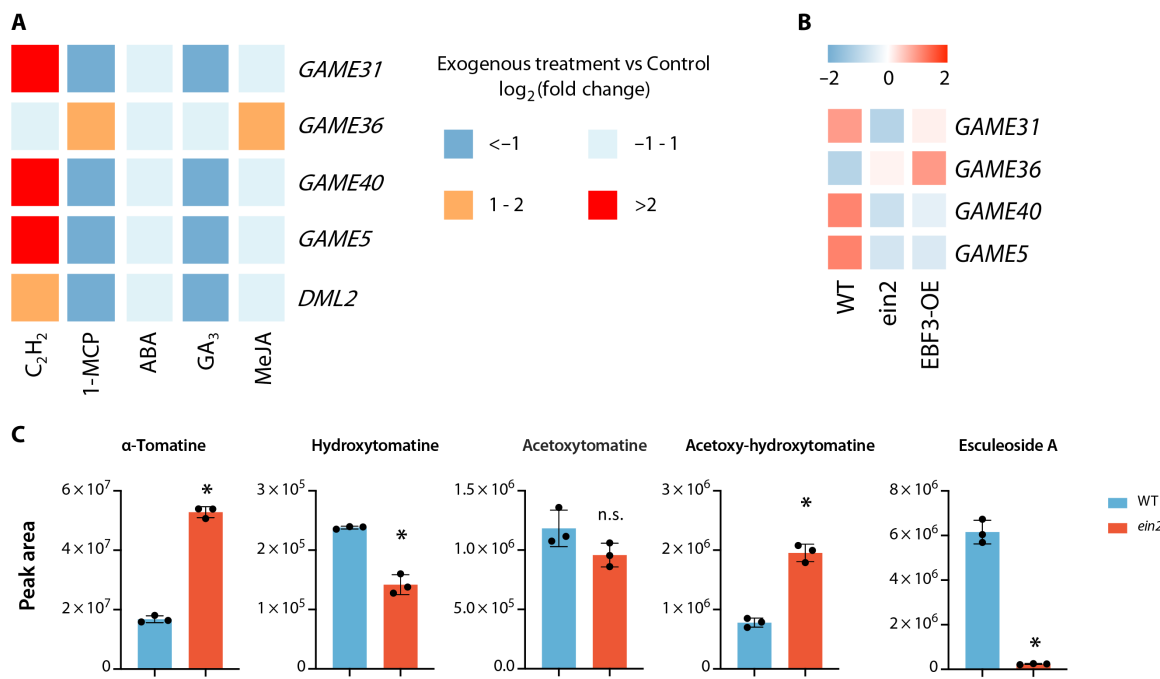


**Fig. 2. Ethylene induces the expression of ripening-related *GAMEs*.** (A) Summarized gene changes in exogenous hormone-treated tomato fruit. Genes that were significantly increased by treatment were colored based on RT-qPCR data. Data were represented as  $\log_2(\text{fold change})$  compared to control. (B) Heatmap representation of the expression of SGA biosynthesis genes in *ein2* and *EBF3-OE* fruits at the red stage based on RT-qPCR data. The values of heatmap were normalized by z score. (C) SGA profiles of WT and *ein2* fruits at the red stage. Data are presented as means  $\pm$  SD ( $n = 3$ ). \* $P < 0.05$  in two-sided t test. n.s., not significant.

ETHYLENE INSENSITIVE 2 (EIN2) and EIN3-BINDING BOX 3 (EBF3) are two key components of the ethylene signal transduction pathway with opposite functions in tomato (32, 33). Knockout of *EIN2* (*ein2*) or overexpression of *EBF3* (*EBF3-OE*) in tomato resulted in ethylene-insensitive tomato plants and a block in fruit ripening (32, 33). To elucidate the critical role of ethylene in modulating SGA conversion during ripening, we assessed the expression levels of the four *GAME* genes in *ein2*, *EBF3-OE*, and WT fruits at the red ripe stage. The expression levels of *GAME31*, *GAME40*, and *GAME5* were significantly down-regulated in both *ein2* and *EBF3-OE* fruits, whereas those of *GAME36* were up-regulated (Fig. 2B). In agreement with this pattern, an analysis of SGA components in *ein2* fruits revealed that the  $\alpha$ -tomatine level was elevated by 3.15 times than that in WT, whereas esculetoside A levels dropped by 96.2% (Fig. 2C). These findings indicate that, in ethylene signaling-deficient lines, the conversion of toxic  $\alpha$ -tomatine is largely blocked, supporting the idea that ethylene is a crucial regulator of SGA metabolism during fruit ripening.

### Key ripening transcriptional regulators control the conversion of toxic and bitter SGAs during fruit ripening

TFs, such as NOR, RIN, and FUL1, are key regulators of fruit ripening by partially modulating the ethylene biosynthesis and signaling pathways (22–24). An analysis of RNA sequencing (RNA-seq) data (34) followed by a clustering analysis showed that the TF genes NOR, RIN, and FUL1 group with the four *GAME* genes *GAME31*, *GAME36*, *GAME40*, and *GAME5* (Fig. 3A), suggesting a positive association between these TF genes and the expression of the four ripening-related *GAME* genes. To investigate the regulatory role of these TFs in SGA metabolism during fruit ripening in more detail, we performed a combined coexpression analysis using transcriptome data for these

key ripening-related TF genes and the ripening-related *GAME* genes together with SGA metabolic data during fruit ripening. All three TF genes were coexpressed with at least one *GAME* gene, and their expression levels were correlated with the abundance of at least one metabolite ( $r$  value  $\geq 0.8$ ) (Fig. 3B). In addition, previous RNA-seq data from knockout lines of *NOR* (*nor*), *RIN* (*rin*), and *FUL1* (*ful1*) and from *FUL1/FUL2* cosuppressed lines (*TF18*) (34–37) showed that the transcript levels of the ripening-associated *GAME* genes *GAME31*, *GAME40*, and *GAME5* (although not *GAME36*) were significantly lower in the fruits of *nor*, *rin*, *ful1*, and *TF18* lines than in WT fruits at red ripe stage (Fig. 3C, fig. S3B, and data S2 and S3), suggesting a positive regulation of the expression of *GAME31*, *GAME40*, and *GAME5* by the three key ripening-related TFs.

To further study how NOR, RIN, and FUL1 modulate the removal of toxic and bitter SGAs during ripening by regulating ripening-associated *GAME* genes, we generated independent *NOR* knockout lines (*NOR-KO*) by clustered regularly interspaced short palindromic repeats (CRISPR)-CRISPR-associated nuclelease 9 (Cas9)-mediated genome editing, new *FUL1/FUL2* cosuppression (*FUL1/2-CS*) lines, and *FUL1* overexpression (35S:*FUL1*-FLAG, *FUL1-OE*) lines (Fig. 3D and fig. S3, C to E). We also obtained knockout lines for *RIN* (*RIN-KO*) from a previous study (37). We then examined the relative expression levels of the three ripening-associated *GAME* genes in these ripening-defective mutants and *FUL1-OE* lines by RT-qPCR. The transcript levels of *GAME31*, *GAME40*, and *GAME5* were all significantly lower in the fruits of *NOR-KO*, *RIN-KO*, and *FUL1/2-CS* lines compared to WT at the red ripe stage (fig. S3F), validating the RNA-seq data (Fig. 3C). The relative expression levels of the three ripening-related *GAME* genes were increased in *FUL1-OE* lines (fig. S3F). These findings indicate that NOR, RIN, and

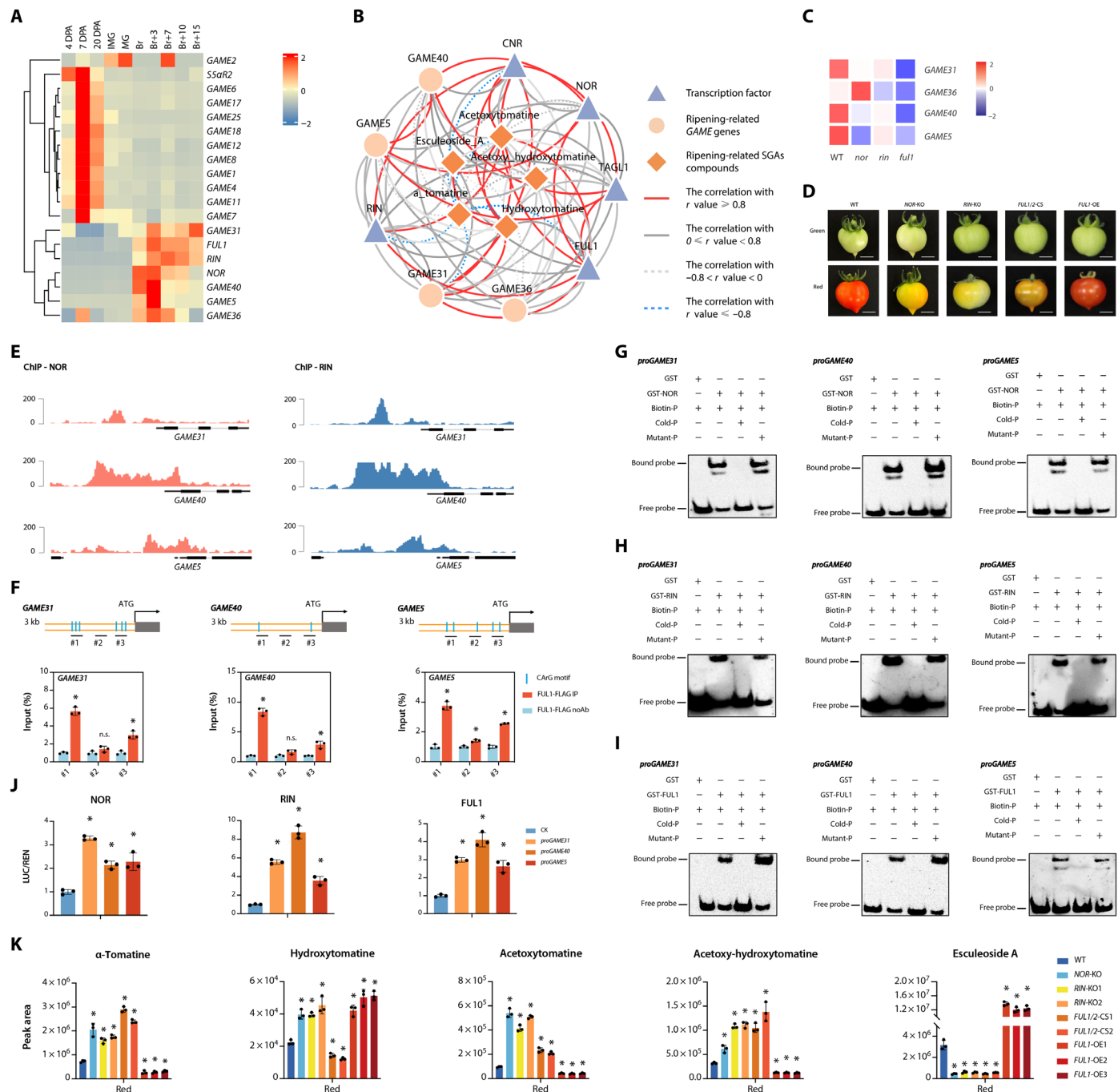


**Fig. 3. NOR, RIN, and FUL1 can bind directly to the GAME genes.** (A) Heatmap representation of the expression patterns of SGA biosynthesis genes and ripening-related TFs. Gene expression was normalized using the min-max method. (B) Coexpression analysis of ripening-related TFs, GAME genes, and SGA compounds. (C) Expression patterns of genes involved in SGA metabolism in three mutants and WT. The values of heatmap were normalized by z score. Red color indicates highest expression, and blue indicates lowest expression. (D) Representative images of WT, NOR-KO, RIN-KO, FUL1/2-CS, and FUL1-OE fruits at green and red stages. Scale bars, 10 mm. (E) ChIP-seq data of NOR and RIN analysis in GAME gene promoters. (F) ChIP-qPCR of FUL1-FLAG levels at the promoters of GAME31, GAME40, and GAME5 in fruits at the red stage. Data are presented as means  $\pm$  SD ( $n = 3$ ). \* $P < 0.05$  in two-sided t test. (G to I) EMSA assays showing the direct binding of NOR (G), RIN (H), and FUL1 (I) to the promoters of three GAME genes via the NACRS or CArG motifs. Biotin-P, the probe labeled with biotin; Cold-P, 100x unlabeled probe; Mutant-P, mutated probe; The symbols – and + represent absence and presence, respectively. (J) Dual-luc assay showing the activation capacity of NOR, RIN, and FUL1 on the promoter of GAME31 (pro-GAME31), GAME40 (proGAME40), and GAME5 (proGAMES). Data are presented as means  $\pm$  SD ( $n = 3$ ). The ordinary one-way ANOVA followed by Dunnett's multiple comparison test was performed to show statistical difference (\* $P < 0.05$ ). (K) SGA profiles of WT, NOR-KO, RIN-KO, FUL1/2-CS and FUL1-OE fruits at the red stage. Data are presented as means  $\pm$  SD ( $n = 3$ ). The ordinary one-way ANOVA followed by Dunnett's multiple comparison test was performed to show statistical difference (\* $P < 0.05$ ).

FUL1 can regulate the expression of *GAME31*, *GAME40*, and *GAME5* during ripening.

To address whether these key ripening-related TFs are involved in the direct regulation of the three ripening-associated *GAME* genes, we mined available chromatin immunoprecipitation sequencing (ChIP-seq) or ChIP-chip data for the three key ripening-related TFs (20, 30). ChIP-seq results revealed clear enrichment for both NOR and RIN at the promoter regions of *GAME31*, *GAME40*, and *GAME5* (Fig. 3E) and a much weaker enrichment at the promoter region of *GAME36* (fig. S3G). We also observed high enrichment of FUL1 over the promoter regions of *GAME31*, *GAME40*, and *GAME5* based on ChIP-chip data (data S4). Using the new *FUL1*-OE lines generated in this study, we validated the binding of FUL1 to the three ripening-related *GAME* genes by ChIP-qPCR assays (Fig. 3F). Moreover, we conducted electrophoresis mobility shift assays (EMSA) using recombinant purified NOR, RIN, and FUL1 fused to glutathione S-transferase (GST) to confirm the direct binding of NOR, RIN and FUL1 to labeled probes derived from the *GAME31*, *GAME40*, and *GAME5* promoters containing an NAC (NAM/ATAF1,2/CUC2) recognition sequence (NACRS; for NOR) or a CArG *cis*-element (MADS recognition sequence; for RIN and FUL1). We detected a shift in the mobility of the labeled intact probes in the presence of each recombinant protein, which was completed by coincubation with an unlabeled intact probe but not by an unlabeled mutated probe (Fig. 3, G to I). To demonstrate the transcriptional regulation of the three ripening-associated *GAME* genes by NOR, RIN, and FUL1, we performed dual-luciferase assays by placing the firefly luciferase (*LUC*) reporter gene under the control of the *GAME31*, *GAME40*, or *GAME5* promoter and using each TF gene expressed from the constitutive cauliflower mosaic virus (CaMV) 35S promoter as effector constructs (fig. S3H). The presence of NOR, RIN, or FUL1 significantly activated *LUC* transcription driven by each promoter tested (Fig. 3J), indicating that the transcription of these *GAME* genes is activated by these TFs. These results demonstrate that the three *GAME* genes *GAME31*, *GAME40*, and *GAME5* are direct targets of NOR, RIN, and FUL1.

We further measured the SGA contents in the fruits of WT, NOR-KO, RIN-KO, *FUL1*/2-CS, and *FUL1*-OE lines using UPLC-MS. At the red ripe stage, the levels of  $\alpha$ -tomatine, hydroxytomatine, acetoxytomatine, and acetoxy-hydroxytomatine were significantly increased whereas that of esculeoside A was markedly lower in NOR-KO and RIN-KO fruits compared to WT fruits (Fig. 3K). Moreover, the levels of  $\alpha$ -tomatine, acetoxytomatine, and acetoxy-hydroxytomatine were significantly lower in *FUL1*-OE fruits but higher in *FUL1*/2-CS fruits than in WT fruits at the red ripe stage. Consistent with these results, the content of nontoxic and nonbitter esculeoside A was higher in *FUL1*-OE fruits and significantly lower in *FUL1*/2-CS fruits compared to WT fruits (Fig. 3K). Together, these data further support the notion that NOR, RIN, and FUL1 play a crucial role in positively regulating the shift in SGA profile from  $\alpha$ -tomatine to esculeoside A during fruit ripening.

### DNA methylation and key ripening-related TFs form a feedback loop that regulates *GAME* genes during fruit ripening

It was previously demonstrated that the NOR genomic region is hypermethylated and its expression is down-regulated during ripening in *dml2* mutant lines (30). Moreover, NOR can activate

*DML2* expression by binding to its promoter (30). This information prompted us to explore the relationship between DNA methylation and key ripening-related TFs in the removal of toxic SGAs during fruit ripening. We determined that the DNA methylation levels at the *NOR*, *RIN*, and *FUL1* loci gradually decrease over the course of fruit ripening from 17 to 52 DPA (Fig. 4A). In the *dml2* mutant, the promoter regions of *NOR*, *RIN*, and *FUL1* showed a higher methylation level than in WT (Fig. 4B). Moreover, the expression of *NOR*, *RIN*, and *FUL1* was down-regulated in *dml2* fruits at the red ripe stage compared to WT (Fig. 4C). These data indicate that *DML2* is necessary for the proper expression of *NOR*, *RIN*, and *FUL1* during ripening.

To gain more insight into their regulatory relationship, we examined *DML2* transcript levels in WT, *NOR*-KO, *RIN*-KO, and *FUL1*/2-CS fruits by RT-qPCR. *DML2* expression was significantly lower in the fruits of *NOR*-KO, *RIN*-KO, and *FUL1*/2-CS lines at red ripe stages (Fig. 4D), suggesting that there is a positive feedback loop between *DML2* and the ripening-related TFs. Because the regulation of *DML2* expression by NOR was previously reported (30), we searched available ChIP-seq data for RIN (Fig. 4E) and performed a ChIP-qPCR assay for FUL1 (Fig. 4F) to validate their respective direct binding to the *DML2* promoter. In addition, EMSAs further confirmed the direct binding of RIN and FUL1 to probes derived from the *DML2* promoter (Fig. 4G).

Because RIN and FUL1 can form a heterodimer that regulates the transcription of their target genes (25), we tested whether this complex plays a role in the transcriptional regulation of *GAME* genes. First, we performed a yeast two-hybrid (Y2H) assay, which confirmed that RIN can heterodimerize with FUL1 in yeast cells (Fig. 4H). We then cotransfected effector constructs overexpressing RIN and/or FUL1 together with the reporter construct *proDML2:LUC*, *proGAME31:LUC*, *proGAME40:LUC*, or *proGAME5:LUC* in *Nicotiana tabacum* protoplasts (Fig. 4I). We obtained significantly higher relative LUC activity for the four above reporter constructs in the presence of the RIN-FUL1 complex than with either RIN or FUL1 alone (Fig. 4J). These results suggest that RIN interacts with FUL1 to positively regulate the transcription of *DML2*, *GAME31*, *GAME40*, and *GAME5* during ripening.

### GORKY expression is under the control of DNA methylation and key ripening regulators

During ripening, GORKY is responsible for the transport of toxic SGAs (especially  $\alpha$ -tomatine) from the vacuole to the cytosolic domain to facilitate the conversion of  $\alpha$ -tomatine to esculeoside A (4). Because GORKY expression increased markedly at the transition to ripening, as is the case for the three ripening-related *GAME* genes (Fig. 5A), we hypothesized that the change in GORKY expression during ripening may also be under the control of DNA methylation and ripening-related TFs. To test this idea, we analyzed the DNA methylation level along the GORKY promoter by mining published methylome sequencing data (20). DNA methylation levels over the GORKY promoter decreased during ripening regardless of cytosine context (Fig. 5B). In the *dml2* mutant, the GORKY promoter was hypermethylated and this gene was transcribed at lower levels than in WT (Fig. 5, C and D). This result suggests that the expression level of GORKY is associated with DNA methylation.

To investigate whether GORKY expression is under the control of ethylene, we performed RT-qPCR using MG fruits treated with

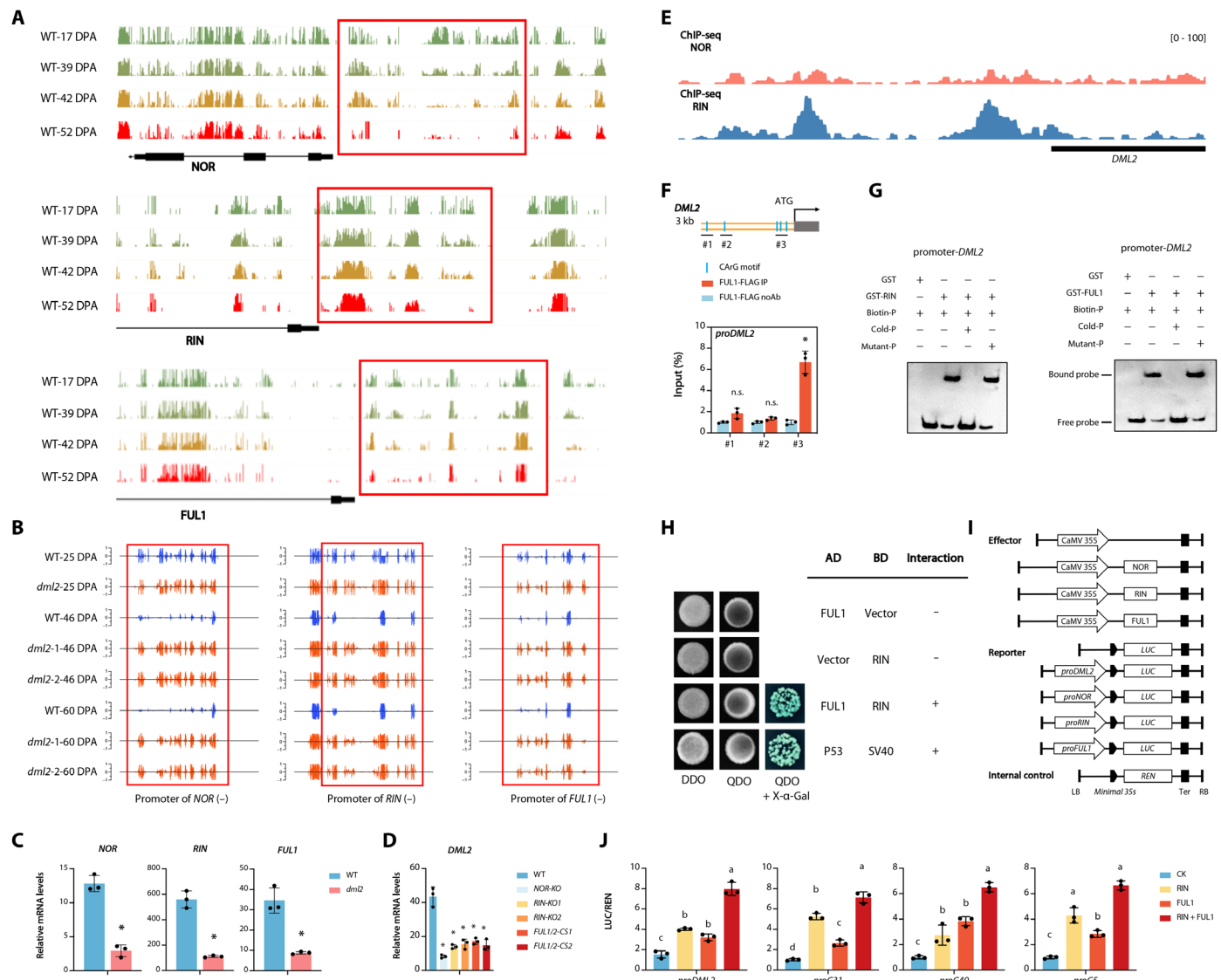


**Fig. 4. Relationship between DNA methylation and TFs in the conversion of SGAs during tomato ripening.** (A) Screenshot of DNA methylation levels of NOR, RIN, and FUL1 promoter at different stages. Red boxed areas are DMRs. (B) Methylation levels of NOR, RIN, and FUL1 promoters in WT and *dml2* mutant fruits at 25-, 46-, and 60-DPA. Red boxed areas are hyper-DMRs. (C) Expression of NOR, RIN, and FUL1 detected by RT-qPCR in WT and *dml2* fruits. Data are presented as means  $\pm$  SD ( $n = 3$ ). \* $P < 0.05$  in two-sided *t* test. (D) Expression of DML2 in WT, NOR-KO, RIN-KO, and FUL1/2-CS fruits at the red stage. Data are presented as means  $\pm$  SD ( $n = 3$ ). \* $P < 0.05$  in ordinary one-way ANOVA followed by Dunnett's multiple comparison test. (E) ChIP-seq data of NOR and RIN analysis in DML2 promoter. (F) ChIP-qPCR of FUL1-FLAG levels at the promoter of DML2 in fruits at the red stage. Data are presented as means  $\pm$  SD ( $n = 3$ ). \* $P < 0.05$  in two-sided *t* test. (G) EMSA assays showing the direct binding of RIN and FUL1 to the promoter of DML2. Biotin-P, the probe labeled with biotin; Cold-P, unlabeled probe; Mutant-P, mutated probe. The symbols – and + represent absence and presence, respectively. (H) Y2H assays between RIN and FUL1. P53 and SV40 vectors were cotransformed as positive controls. (I) Schematic illustration of the reporter and effector plasmid used in the dual-luc assays. (J) Dual-luc assays showing the activation capacity of RIN and FUL1 on the promoters of target genes. Data are presented as means  $\pm$  SD ( $n = 3$ ). There are significant differences between pairwise samples indicated by the lowercase letters a, b, or c above each of the bars. \* $P < 0.05$  in one-way ANOVA with Tukey's multiple comparison test.

ethylene or Br fruits treated with 1-MCP. Relative GORKY transcript levels were significantly increased in response to ethylene treatment (Fig. 5E) and decreased by about 96% in response to 1-MCP (Fig. 5F). Furthermore, GORKY expression was significantly down-regulated in fruits from the ethylene signaling-deficient *ein2* mutant and *EBF3*-OE line (Fig. 5G). Collectively, these findings provide strong evidence that GORKY expression is positively regulated by ethylene.

To decipher the transcriptional regulation of GORKY, we examined published RNA-seq data for the *nor*, *rin*, and *ful1* mutants, which showed that GORKY transcript levels are lower in these mutants than in WT (Fig. 5D). These data are consistent with the decreased expression levels of GORKY gene in NOR-KO, RIN-KO, and FUL1/2-CS lines (Fig. 5H). We determined that RIN and FUL1 directly bind to the GORKY promoter through ChIP-seq and ChIP-qPCR experiments, respectively (Fig. 5, I and J). By contrast, NOR

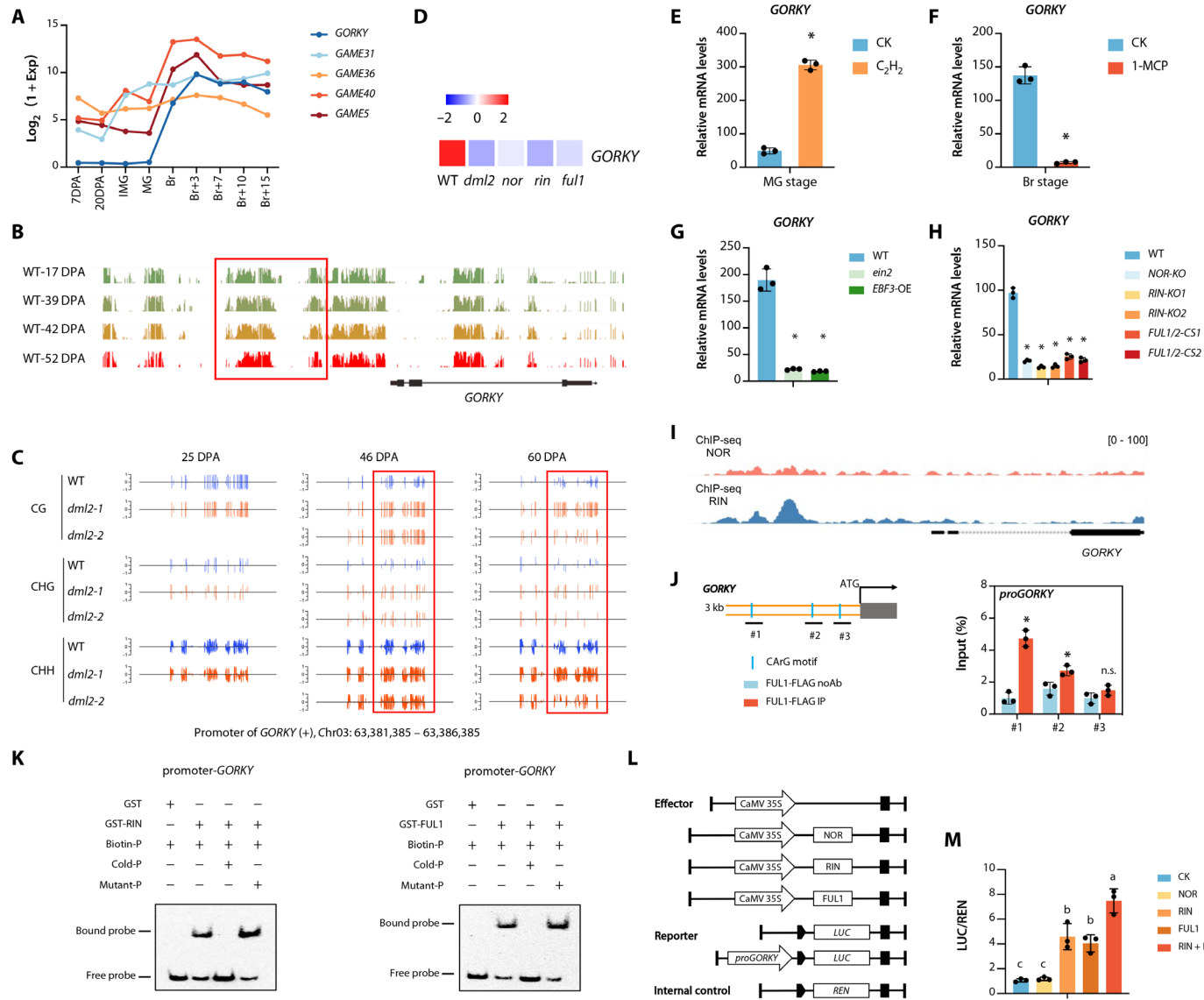


**Fig. 5. The expression of GORKY was regulated by the regulatory network during ripening.** (A) Expression data of GORKY and four *GAME* genes during fruit ripening. (B) Screenshot of DNA methylation levels of GORKY promoter at different stages. Red boxed areas are DMRs. (C) Methylation levels of GORKY promoter in WT and *dml2* fruits at 25-, 46-, and 60-DPA. Red boxed areas are hyper-DMRs. (D) Expression pattern of GORKY in WT and four mutants. (E and F) Relative transcript levels of GORKY in WT fruits treated with ethylene or 1-MCP. Data are presented as means  $\pm$  SD ( $n = 3$ ). \* $P < 0.05$  in two-sided *t* test. (G) Expression of GORKY in WT, *ein2*, and *EBF3*-OE fruits. Data are presented as means  $\pm$  SD ( $n = 3$ ). \* $P < 0.05$  in ordinary one-way ANOVA followed by Dunnett's multiple comparison test. (H) Expression of GORKY in WT, *NOR*-KO, *RIN*-KO, and *FUL1/2-CS* fruits. Data are presented as means  $\pm$  SD ( $n = 3$ ). \* $P < 0.05$  in ordinary one-way ANOVA followed by Dunnett's multiple comparison test. (I) ChIP-seq data analysis of NOR and RIN in GORKY promoter. (J) ChIP-qPCR of *FUL1*-FLAG levels at the promoter of GORKY. Data are presented as means  $\pm$  SD ( $n = 3$ ). \* $P < 0.05$  in two-sided *t* test. (K) EMSA assays showing the direct binding of RIN and FUL1 to the promoter of GORKY. (L) Schematic illustration of the reporter and effector plasmid used in the dual-luc assays. (M) Dual-luc assays showing the activation capacity of NOR, RIN, and FUL1 on the promoters of GORKY. Data are presented as means  $\pm$  SD ( $n = 3$ ). There are significant differences between pairwise samples indicated by the lowercase letters a, b, or c above each of the bars. \* $P < 0.05$  in ordinary one-way ANOVA followed by Tukey's multiple comparison test.

did not show direct binding to the GORKY promoter based on ChIP-seq, despite the down-regulation of GORKY in the *nor* mutant (Fig. 5I). We validated the direct binding of recombinant purified RIN and FUL1 tagged with GST to CArG *cis*-elements present in the GORKY promoter by EMSAs (Fig. 5K). We also performed a dual-luciferase assay to test the transcriptional transactivation activity of RIN and FUL1 toward the GORKY promoter, using a *pro*GORKY:LUC reporter construct (Fig. 5L). We detected a significant activation of

*proGORKY:LUC* transcription by RIN or FUL1, whereas NOR failed to activate transcription from the *GORKY* promoter (Fig. 5M). Moreover, cotransfection of *RIN* and *FUL1* resulted in a significantly higher induction of *LUC* transcription from the *GORKY* promoter compared to *RIN* or *FUL1* alone (Fig. 5M). Together, these results support the notion that RIN and FUL1 coregulate the conversion from toxic  $\alpha$ -tomatine to esculenoside A during ripening by regulating the expression of *GORKY* through binding to its promoter.

## MYC2 acts as a key regulator of SGA conversion by modulating GAME36 expression

*GAME31*, *GAME36*, *GAME40*, and *GAME5* are the four genes encoding the enzymes responsible for the conversion of toxic and bitter  $\alpha$ -tomatine to esculetoside A. However, in contrast to the other three ripening-associated *GAME* genes (*GAME31*, *GAME40*, and *GAME5*), *GAME36* was not induced by ethylene or key ripening-associated TFs, as evidenced by ChIP-seq data for each TF (Fig. 2A and fig. S3G). The

induction of *GAME36* by MeJA treatment prompted us to investigate the possible regulation of *GAME36* by the JA signal pathway and plays a critical role in SGA metabolism (12, 38, 39), we examined *GAME36* expression in a knockout line of MYC2 (*myc2*). *GAME36* expression was down-regulated in *myc2* fruits compared to WT (Fig. 6A). Moreover, treatment of *myc2* with MeJA failed to induce *GAME36* expression (Fig. 6A). These results suggested that

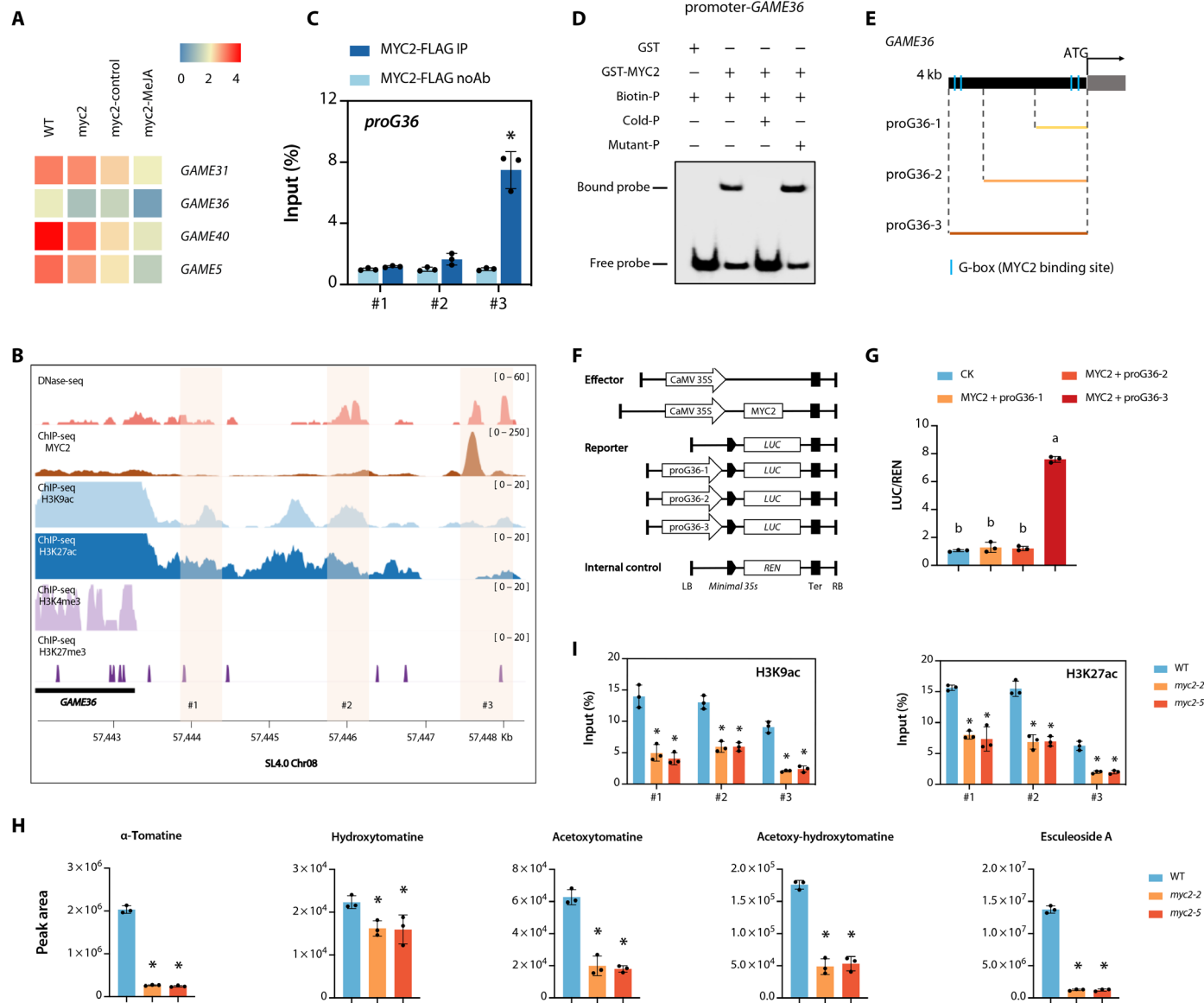


**Fig. 6. MYC2 coordinates transcriptional and epigenetic regulation of *GAME36*.** (A) Heatmap representation of the expression of SGA biosynthesis genes in WT and *myc2*. Data were represented as  $\log_2(\text{expression})$ . (B) DHS and histone modifications profiles in the promoter of *GAME36*. Three regions (#1 to #3) were three sites used for ChIP-qPCR assay. (C) ChIP-qPCR of MYC2-FLAG levels at the promoter of *GAME36* in fruits at the red stage. Data are presented as means  $\pm$  SD ( $n = 3$ ). \* $P < 0.05$  in two-sided  $t$  test. (D) EMSA assays showing the direct binding of MYC2 to the promoter of *GAME36*. Biotin-P, the probe labeled with biotin; Cold-P, unlabeled probe; Mutant-P, mutated probe. The symbols – and + represent absence and presence, respectively. (E) Schematic diagram of three fragments used in dual-luc assays. (F) Schematic illustration of the reporter and effector plasmid used in the dual-luc assays. (G) Dual-luc assays showing the activation capacity of MYC2 on the promoter of *GAME36*. Data are presented as means  $\pm$  SD ( $n = 3$ ). There are significant differences between pairwise samples indicated by the lowercase letters a or b above each of the bars. \* $P < 0.05$  in one-way ANOVA with Tukey's multiple comparison test. (H) SGA profiles of WT, *myc2-2*, and *myc2-5* fruits at the red stage. Data are presented as means  $\pm$  SD ( $n = 3$ ). The ordinary one-way ANOVA with Dunnett's multiple comparison test was performed to show statistical difference (\* $P < 0.05$ ). (I) ChIP-qPCR analysis of H3K9ac and H3K27ac levels at #1 to #3 of *GAME36* promoter in WT and *myc2* fruits at the red stage. Data are presented as means  $\pm$  SD ( $n = 3$ ). \* $P < 0.05$  in ordinary one-way ANOVA with Dunnett's multiple comparison test.

MYC2 contributes to the regulation of *GAME36* expression and that the induction of *GAME36* by JA is dependent on MYC2. Further analysis of published ChIP-seq data revealed that MYC2 is enriched at the promoter region of *GAME36* (~4 kb upstream of the ATG), a region that has high chromatin accessibility (Fig. 6B). By contrast, MYC2 was not enriched at the promoter regions of the other three *GAME* genes (fig. S4). ChIP-qPCR analysis using MYC2 overexpression lines (*MYC2-FLAG*) with an anti-FLAG antibody confirmed that MYC2 was significantly enriched over region #3 of the *GAME36* promoter (Fig. 6C). In addition, an EMSA demonstrated the direct binding of recombinant purified GST-MYC2 to the *GAME36* promoter (Fig. 6D).

To further investigate the activation capacity of *GAME36* transcription by MYC2, we conducted a dual-luciferase reporter assay with different *GAME36* promoter fragments encompassing region #1 alone (*proGAME36-1*, 1.5 kb), regions #1 and #2 (*proGAME36-2*, 3 kb), or regions #1, #2, and #3 (*proGAME36-3*, 4 kb) (Fig. 6E). MYC2 activated only *LUC* transcription driven by the longest promoter fragment, *proGAME36-3*, but not by the two shorter promoter fragments (Fig. 6, F and G). This finding is consistent with the ChIP-seq and ChIP-qPCR data (Fig. 6, B and C) and suggests that MYC2 directly regulates *GAME36* transcription through the two G-boxes located ~4 kb upstream of the ATG of the gene, rather than through the two G-boxes located closer to the ATG.

We then used UPLC-MS to assess the contents of SGA metabolites in fruits from two *myc2* knockout lines (*myc2-2* and *myc2-5*). All five detected SGAs were significantly less abundant in the *myc2* mutants, with hydroxytomatine showing a more modest drop in abundance than the other four compounds (*GAME36* catalyzes the conversion of hydroxytomatine to acetoxytomatine) (Fig. 6H). These findings suggest that MYC2 mediates SGA conversion during ripening through regulation of *GAME36* expression.

A previous study highlighted a strong association between MYC2-mediated transcriptional regulation and histone modifications, particularly histone acetylation (40). We thus opted to analyze histone modifications over the *GAME36* locus, which revealed significant enrichment for the H3K9ac and H3K27ac marks along the gene body and promoter regions, with no clear enrichment for H3K4me3 or H3K27me3 (Fig. 6B). This finding suggests that H3K9ac and H3K27ac may be involved in MYC2-mediated regulation of *GAME36* transcription. Accordingly, we assessed H3K9ac and H3K27ac levels in WT and the *myc2-2* and *myc2-5* mutants. We observed a significant decrease in acetylation levels at three specific sites (#1 to #3) in the two knockout lines compared to WT (Fig. 6I). Collectively, these results indicate that MYC2 regulates *GAME36* transcription by affecting the histone acetylation levels of its promoter region.

### Removal of toxic SGAs and bitterness during ripening was under selection during tomato domestication

The contents of SGA were reported to have been under negative selection during tomato domestication from *Solanum pimpinellifolium* (PIM) to *S. lycopersicum* var. *cerasiforme* (CER) and ultimately to *S. lycopersicum* (BIG) (41). We therefore analyzed the contents of five SGAs (α-tomatine, esculeoside A, and the three intermediate compounds hydroxytomatine, acetoxytomatine, and acetoxyhydroxytomatine) and the expression of genes related to the conversion of toxic α-tomatine to nontoxic esculeoside A in 342 tomato accessions consisting of 23 PIM accessions, 71 CER accessions, and 248 BIG accessions (41–43). The contents of hydroxytomatine and acetoxytomatine were comparable between PIM and CER accessions, whereas

the contents of α-tomatine, acetoxy-hydroxytomatine, and esculeoside A decreased (Fig. 7A). The levels of all five compounds decreased in BIG accessions relative to CER accessions, supporting a negative selection for SGAs during tomato domestication (Fig. 7A). Notably, whereas *GAME36* expression declined from PIM accessions to CER and then BIG accessions (Fig. 7B), the expression levels of *GAME31*, *GAME40*, *GAME5*, and *GORKY* showed a common pattern of a decrease in CER accessions relative to PIM accessions, followed by an increase in BIG accessions compared to CER accessions (Fig. 7B). The different expression changes of *GAME* genes and *GORKY* suggest that these genes may have differentially contributed to the selection of SGA contents from PIM to CER accessions and from CER to BIG accessions during domestication. Moreover, the increased expression levels of the three *GAME* genes and *GORKY* in BIG accessions compared to CER accessions suggest that the conversion from toxic α-tomatine to nontoxic esculeoside A increased during domestication. Furthermore, *DML2* expression was highly correlated with that of *GAME31*, *GAME40*, *GAME5*, and *GORKY*, whereas MYC2 expression level was correlated with that of *GAME36* (Fig. 7B), which is consistent with the specific regulation of *GAME36* by MYC2. These data suggest that *DML2* and MYC2 have key roles in modulating the removal of toxic SGAs during domestication. Notably, the trends in *NOR* and *RIN* up-regulation in BIG versus CER accessions (Fig. 7B) are consistent with the increased transcript levels of the three ripening-related *GAME* genes and of *GORKY* during tomato domestication in the same sets of accessions, further supporting the likelihood that *GAME31*, *GAME40*, *GAME5*, and *GORKY* are regulated by these TFs. To validate these findings, we analyzed the genomic positions of these genes and found that *DML2*, *MYC2*, *NOR*, *FUL1*, *GAME5*, and *GAME36* are located within the domestication sweeps (fig. S5, A to C) (42, 43). The overlaps between these genes and the domestication sweeps support their contribution to the removal of toxic SGAs during tomato domestication.

An analysis of 46 tomato genomes (42, 43), representative of the PIM, CER, and BIG groups, uncovered a *DML2* allelic variant with a 13-base pair (bp) deletion in the third intron (fig. S5D and data S5). The frequency of this variant, named *DML2<sup>13D</sup>*, declined across domestication stages from PIM to CER to BIG (Fig. 7, C and D). Furthermore, publicly available RNA-seq data indicated that the expression levels of *DML2* and the three ripening-related *GAME* genes in 18 accessions (four with *DML2<sup>13D</sup>* and 14 with *DML2*) were significantly lower in accessions harboring the *DML2* allele than in those with the *DML2<sup>13D</sup>* variant (Fig. 7E). On the basis of these findings, we hypothesize that the *DML2<sup>13D</sup>* allele was subjected to negative selection during domestication from PIM to CER accessions, leading to decreased levels of toxic SGAs.

### DISCUSSION

*Solanaceae* crops such as tomato produce toxic SGAs to protect themselves from attacks by pests and animals during plant and fruit development; these toxic SGAs must be removed during fruit ripening to make fruits more edible and palatable, thus facilitate seed dispersal by enticing animals as the vector (44). Thus, the precise regulation of SGA metabolism is vital to the balance between defense during development and the development of tasty ripe fruits. Although great progress has been achieved in understanding SGA metabolism through the identification of key structural genes and

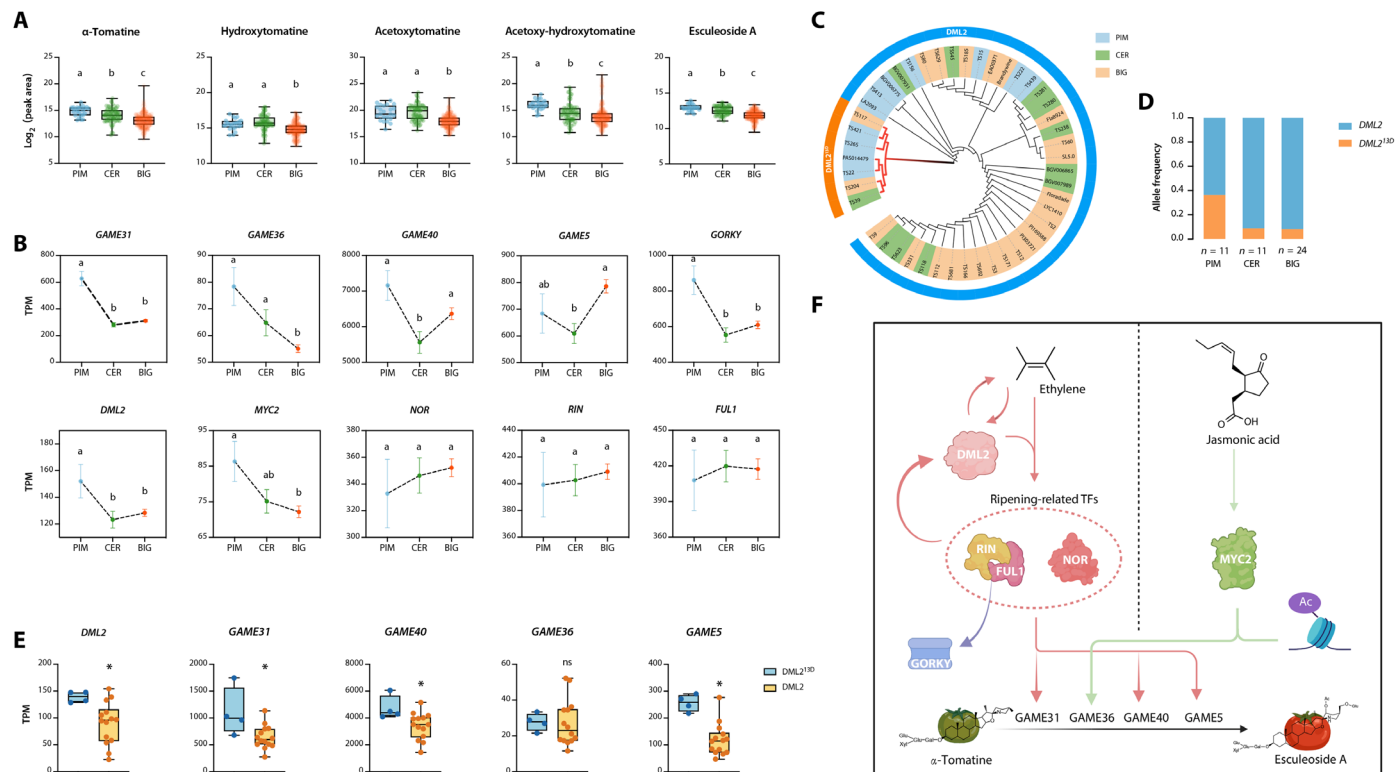


**Fig. 7. Domestication selects metabolic modules for toxic SGA removal in tomato.** (A) Analysis of five SGA contents pathway across 342 accessions. Dots indicate individual tomato accession. There are significant differences between pairwise accessions indicated by the lowercase letters a, b, or c above each of the graphics. The one-way ANOVA with Tukey's multiple comparison test was performed to show statistical difference ( $*P < 0.05$ ). (B) Analysis of expression levels of 10 genes related to the SGA pathway across 342 accessions ( $n_{PIM} = 23$ ,  $n_{CER} = 71$ , and  $n_{BIG} = 248$ ). Dots indicate individual tomato accession. There are significant differences between pairwise accessions indicated by the lowercase letters a, b, or ab above each of the variation bars. Different lowercase letters indicate significant changes. The one-way ANOVA with Tukey's multiple comparison test was performed to show statistical difference ( $*P < 0.05$ ). (C) Phylogenetic tree of 46 accessions, which was constructed with full-length of *DML2* by using RAXML software (100 times bootstrap) and GTRGAMMA model parameters. (D) Allele frequencies of *DML2* in three groups. Data are presented as percentage of *DML2* by in each group. *n*, tomato accession numbers in group; PIM, *S. pimpinellifolium*; CER, *S. lycopersicum* var. *cerasiforme*; BIG, *S. lycopersicum*. (E) Five genes detected in 18 varieties. Dots indicate individual tomato accession, and data are presented as means  $\pm$  SEM ( $n_{DML2^{3D}} = 4$ ;  $n_{DML2} = 14$ ).  $*P < 0.05$  in two-sided t test. (F) Model of DNA methylation, ethylene, and TF regulation of the shift in SGA profiles during ripening. At the green stage, the expression of the target genes is extremely low due to hypermethylation and low ethylene production. During ripening, the decreased DNA methylation and increased ethylene drive the conversion of  $\alpha$ -tomatine to esculetoside A.

associated metabolic pathways (1, 2, 6, 9–11), the regulatory network governing the conversion from toxic and bitter  $\alpha$ -tomatine to nontoxic and nonbitter esculetoside A has remained poorly understood. Here, we demonstrate that this conversion during ripening is coordinately regulated by epigenetic modifications such as DNA methylation and histone acetylation, the plant hormones ethylene and JA, and the TFs RIN, NOR, FUL1, and MYC2 (Fig. 7F). Moreover, our findings reveal a regulatory network in which DNA demethylation, ethylene, and TFs form a feedback loop to control the elimination of toxic SGAs and bitterness from tomato fruits during ripening by modulating the expression of *GAME* genes (Fig. 7F). In addition, this detoxification step was under selection during tomato domestication. The results of this study not only advance our understanding of SGA metabolism but also shed light on possible future avenues for *Solanaceae* crop breeding to balance resistance and quality by fine-tuning SGA contents.

We demonstrated that key regulators involved in the conversion of toxic SGAs during ripening, including *DML2*, ethylene, and TFs, are also master factors controlling typical aspects of ripening such as fruit softening and carotenoid biosynthesis (23, 45), indicating that

removal of toxic and bitter SGAs is also a hallmark of ripening. The coregulation of the removal of toxic and bitter SGAs and other ripening hallmarks, such as pigment formation and fruit softening, help ensure that high levels of toxic SGAs remain in immature fruits to maintain resistance against herbivory attacks, guaranteeing that the fruits reach the seed maturation stage. Once seeds are mature, fruits can be made more appealing and palatable through simultaneous accumulation of carotenoids and nontoxic and nonbitter esculetoside A during fruit ripening to facilitate seed dispersal. It is worth pointing out that, because the regulation of fruit ripening and SGA conversion during ripening partially share common mechanisms, our results also extend the ripening regulatory network by demonstrating the feedback regulation of *DML2* expression by RIN and FUL1, which had not previously been reported.

Recently, various TFs involved in the regulation of SGA metabolism have been identified in tomato (12, 13, 33, 38, 39, 45–47). However, most previous studies have focused on the regulation of  $\alpha$ -tomatine accumulation in green fruits, with relatively limited attention devoted to the compound's conversion to esculetoside A during fruit ripening. In the present study, we revealed that the key ripening regulators NOR, RIN,

and FUL1 are key TFs that control the removal of toxic and bitter SGAs by directly regulating the transcription of three *GAME* genes (*GAME31*, *GAME40*, and *GAME5*), encoding enzymes catalyzing the conversion of  $\alpha$ -tomatine to esculenoside A, and *GORKY*, encoding a transporter responsible for the transfer of toxic SGAs from vesicles to the cytosol (4). Moreover, we found that the TF MYC2, normally involved in the JA pathway, acts as an important regulator in this detoxification and bitterness removal by modulating the expression of *GAME36*, encoding another enzyme determining the conversion of SGAs during fruit ripening in tomato. Notably, MYC2 also plays a crucial role in SGA metabolism during fruit development at the green stage (12, 38, 39), suggesting that MYC2 may act as a key TF to balance SGA metabolism across fruit development and ripening.

The contents of  $\alpha$ -tomatine and its downstream compounds decreased in BIG accessions relative to wild PIM accessions, supporting the hypothesis that SGA metabolism was under negative selection during tomato domestication (41, 42). The strong correlation between *DML2* expression and the key *GAME* genes involved in SGA conversion during ripening further suggests that *DML2* was a central regulator driving this selection during domestication. Moreover, the shift in the frequency of the *DML2*<sup>13D</sup> allele, coupled with the altered expression of *DML2* and related *GAME* genes from PIM to BIG accessions, highlights the critical role of *DML2* in SGA detoxification, thereby enhancing the safety and palatability of domesticated tomatoes. During domestication from CER to BIG accessions, the down-regulation of *GAME* gene expression acting upstream of  $\alpha$ -tomatine contributed to the negative selection of total SGA contents (41), whereas the up-regulation of downstream *GAME* genes and *GORKY* promoted  $\alpha$ -tomatine conversion, suggesting that these detoxification genes were under positive selection, driving the evolutionary shift toward nontoxic, palatable tomatoes.

In summary, our study contributes to a deeper understanding of how SGA metabolites undergo dynamic changes at different stages of fruit development and ripening, resulting in nontoxic, edible, and palatable tomato fruits. This greater knowledge of the regulatory mechanisms underlying this metabolic stage opens a fresh avenue to improve fruit nutrient quality, without altering other organoleptic traits, through molecular breeding.

## MATERIALS AND METHODS

### Plant materials

Tomato plants (*S. lycopersicum*) cultivars MicroTom and Ailsa Craig were grown in insect-free greenhouse at ambient temperatures (23°C day/20°C night) under 50% relative humidity and 250 mol m<sup>-2</sup> s<sup>-1</sup> intensity light, according to a 14-hour/10-hour light/night cycle. Seeds of tomato mutant *dml2* in the cv. MicroTom background were kindly provided by Z. Lang (Southern University of Science and Technology, China). Seeds of tomato mutant *RIN*-KO in the cv. Ailsa Craig background were kindly provided by B. Zhu and S. Li (China Agricultural University, China).

### WGBS and analysis

The WGBS data of WT at 17-, 39-, 42-, and 52-DPA from the fruit ENCODE database. The WGBS data of *dml2* and WT at 25- and 46-DPA from the National Center for Biotechnology Information (NCBI) database under Gene Expression Omnibus (GEO) accession number GSE193170 (data S3).

For data analysis, the WGBS reads were fed into fastp v0.22.0 (48) to adapter trimming, low-quality read ( $q < 20$ ) removals, and short-read deletion. Next, the clean reads were mapped to the reference genome using BWA 0.7.17 (49), allowing two mismatches. The reference genome version is SL4.0 ([https://solgenomics.net/ftp/genomes/Solanum\\_lycopersicum/assembly/build\\_4.00/S\\_lycopersicum\\_chromosomes.4.00.fa](https://solgenomics.net/ftp/genomes/Solanum_lycopersicum/assembly/build_4.00/S_lycopersicum_chromosomes.4.00.fa)). The potential PCR duplicates were removed by BWA 0.7.17. DMRs were identified using the method described in refs. (21, 30). Notably, the cytosines with at least 4 $\times$  coverage in all libraries were considered. To identify DMRs, a sliding window approach was used with a 200-bp window that slides at 50-bp intervals. Fisher's exact test was conducted to compare methylated and unmethylated cytosines for each context within each window. False discovery rates (FDRs) were estimated using a Benjamini-Hochberg adjustment of Fisher's *P* values calculated in the R studio. Windows with an FDR of 0.05 or less were selected for further analysis. Any windows within 100 bp of each other were combined into larger regions. The region was then adjusted to narrow down to the first and last differentially methylated cytosines (DMCs). A cytosine was considered differentially methylated if its methylation percentage changed at least twofold. These regions were lastly filtered to include only those with at least 10 DMCs and an arithmetic mean of all cytosine methylation percentages that changed at least twofold.

### ChIP-seq data analysis

The DNase-seq data and ChIP-seq data of NOR, RIN, MYC2, and histone from the NCBI database under BioProject accession numbers PRJNA309352, PRJNA381300, SRA046131, and PRJNA375842, respectively (20, 30, 39). For ChIP-seq data analysis (38), the raw sequencing reads were cleaned by removing bases that had low quality scores ( $q < 20$ ) and removing sequencing adaptors by fastp v0.22.0 and filtering out short reads. The cleaned reads were mapped to the reference genome SL4.0 ([https://solgenomics.net/ftp/genomes/Solanum\\_lycopersicum/assembly/build\\_4.00/S\\_lycopersicum\\_chromosomes.4.00.fa](https://solgenomics.net/ftp/genomes/Solanum_lycopersicum/assembly/build_4.00/S_lycopersicum_chromosomes.4.00.fa)) using BOWTIE2 v.2.4.4 (50) with default settings. MACS2 was used to call peaks in the ChIP-seq datasets (51). The peaks of ChIP-seq data were visualized by pyGenomeTracks (52, 53).

### RNA-seq analysis

Transcriptome profiling was performed as described in ref. (45). The RNA-seq data of *dml2* from the NCBI database under GEO accession number GSE196474. The RNA-seq data of NOR-KO, RIN-KO, and FUL1-KO from the NCBI database under BioProject accession number PRJNA973565. The RNA-seq data of FUL1/FUL2-suppressed transgenic line from the NCBI database under GEO accession numbers GSE49289 and GSE49125. All the RNA-seq data can be found in data S4.

For obtaining clean, high-quality data, quality control of raw data from the Illumina HiSeq 2000 platform was checked using FastQC ([www.bioinformatics.babraham.ac.uk/projects/fastqc](http://www.bioinformatics.babraham.ac.uk/projects/fastqc)) (52, 53). RNA-seq reads were fed into fastp v0.22.031 to adapter trimming, low-quality read removals, and short-read deletion. Next, the clean data were aligned to the tomato reference genome (SL4.0; [https://solgenomics.net/ftp/genomes/Solanum\\_lycopersicum/assembly/build\\_4.00/S\\_lycopersicum\\_chromosomes.4.00.fa](https://solgenomics.net/ftp/genomes/Solanum_lycopersicum/assembly/build_4.00/S_lycopersicum_chromosomes.4.00.fa)). The clean reads were then aligned against the tomato reference genome using HISAT2 v2.2.134 with default parameters (54). Next, uniquely mapped reads with MAPQ > 15 was obtained by Samtools v1.1335 to further analysis. For each gene, featureCounts counted mapped reads and calculated transcripts per million (TPM).

### RNA isolation and RT-qPCR

According to the manufacturer's instructions, total RNA from fruit at green and red stages during ripening was extracted using Plant RNA Purification Reagent (Invitrogen, Waltham, MA, USA; 12322-012). One thousand nanograms of total RNA was used for the first strand of cDNA using the Omniscript Reverse Transcription Kit (Takara, Shiga, Japan; RR047). Gene-specific oligonucleotides were designed with Primer Express software (PE-Applied Biosystems, Waltham, MA, USA). The RT-qPCR was conducted following the protocol outlined in (55), using the Bio-Rad CFX384 Real-Time PCR System (Bio-Rad, Hercules, CA, USA) with SYBR Green qPCR Mix (Vazyme, Nanjing, China; Q431-02). Each sample was analyzed using three independent biological replicates. The data were analyzed using the comparative threshold cycle method ( $\Delta\Delta Ct$ ). Actin (Solyc11g005330) gene was used as internal control.

### Ethylene and 1-MCP treatments at different stages

WT tomato fruits attached to plants at MG and Br stages were placed in sealed boxes and treated with ethylene (50  $\mu$ l liter $^{-1}$ ) or 1-MCP (1.0  $\mu$ l liter $^{-1}$ ) for 24 hours. The pericarps of the fruits were collected and immediately frozen in liquid nitrogen and stored at -80°C until they were used. Total RNA was extracted from fruit pericarps, and RT-qPCR was performed as described previously (55). The primer sequences used in this study are listed in data S6.

### Construction of plasmids and plant transformation

To construct plasmids 35S::*FUL1*, the coding sequences of *FUL1* with a 3xFLAG were cloned into the pBI121 vector under the control of the CaMV 35S promoter. The NOR CRISPR-Cas9 constructs were cloned into the pFASTCas9/ccdB binary vector by a GoldenBraid cloning system under the control of the *Arabidopsis* U6-26 consensus promoter. Guide RNAs were designed using the CRISPR-P v.2.0 online tool (<http://crispr.hzau.edu.cn/cgi-bin/CRISPR2/CRISPR>).

The final constructs pBI121-*FUL1*-FLAG and pFASTCas9/ccdB-NOR were transformed into the tomato cultivar MicroTom via *Agrobacterium*-mediated transformation. The *FUL1*/2-CS lines were serendipitously obtained by overexpression of *FUL1*. Transgenic plant inheritance was stable until the T<sub>2</sub> generation in both overexpression lines and homozygous mutants, allowing for further analysis. All primers used in this study are listed in data S6.

### Sample extraction and metabolomics analysis

Preparation of extracts and the profiling of SGAs in the tomato fruits were performed as described previously (33, 37, 56). Samples were first freeze dried and ground to a fine powder using an automated sample rapid mill (50 Hz, 1 min, repeated three times). Extract 0.1 g of freeze-dried tissue with 1 ml of 80% methanol containing 0.1% formic acid (1:10 weight/volume ratio). Vortex vigorously for 30 s, sonicate at 4°C for 30 min, then vortex again for 30 s, and centrifuge at 20,000g for 10 min. The supernatant was collected and analyzed on a SCIEX Triple Quad 5500 LC-MS/MS system after filtration through a 0.22- $\mu$ m polytetrafluoroethylene membrane filter. The UPLC-MS column of the system was connected online to a Shimadzu photodiode array detector to separate metabolites and detect the mass of eluted compounds. The experiment was conducted as described in ref. (56), with the use of mobile phases A and B, a specified column temperature, a particular solvent flow rate, and an injection volume. The experiment was conducted in biological triplicate. The  $\alpha$ -tomatine used as a standard.

### Dual-luciferase report assays

The transcriptional activity assay was performed as described in ref. (57) with modifications. The effector constructs were generated by amplifying the coding sequences of NOR, RIN, and FUL1 without stop codon and separately insert into the pGreenII 62sk vector with CaMV 35S promoter. For the transactivation assays to test the regulation of NOR, RIN, and FUL1 on the *GAME31*, *GAME36*, *GAME40*, *GAME5*, *DML2*, NOR, RIN, and *FUL1* promoters, each relevant promoter fragment was cloned into the *PGL3* vector with minimal promoter 35S (mp35S)-driven luciferase (*LUC*). *pRL-null* vector was used as the internal control, which had the mp35S-driven Renilla Luciferase (*REN*).

*Nicotiana benthamiana* seeds were sown and cultivated in a culture room at 28°C for 20 to 30 days. The leaves were then harvested to isolate mesophyll protoplasts. Transfection was carried out following the procedure as described previously (38, 57). Dual-luciferase detection was performed ~14 to 16 hours after transfection, according to the instructions provided in the manual for the Dual-Luciferase Reporter Assay System E1960 (Promega, Madison, WI, USA; E1910). Three independent biological replicates and two technological replicates were performed for each assay.

### Electrophoretic mobility shift assays

The full coding sequence of NOR, RIN, and FUL1 were amplified from MicroTom and then inserted into the *pGEX-4 T-1* vector to produce NOR-GST, RIN-GST, and FUL1-GST fusion proteins. The GST-tagged recombinant fusion protein was expressed in Trans BL21 and Rosetta (DE3) *Escherichia coli* cells (Transgene, Beijing, China). After treatment with 0.1 mM isopropyl- $\beta$ -D-thiogalactopyranoside for 14 hours at 18°C, affinity purification was performed with glutathione Sepharose 4B (GE Healthcare, Chicago, IL, USA) according to the manufacturer's instructions. SDS-polyacrylamide gel electrophoresis (PAGE) (10%) was used to detect the purified proteins. The probes containing an NACRS ([TGA][ACG]CGT[GA][TA]) and CArG motif (MADS recognition sequence, C[A/T]<sub>8</sub>G) were synthesized with a 3'-biotin label and annealed to form double-stranded oligonucleotides. The unlabeled DNA fragment was used as competitor, and the mutated probes had the variant NACRS or CArG motif element that had been changed to AAAA or AAAA. The purified proteins (~30 ng of fusion protein per reaction) were incubated with probes in a binding buffer [10 mM tris-HCl (pH 7.2), 50 mM KCl, 1 mM dithiothreitol (DTT), 2.5% glycerol, 0.05% NP-40, and polydeoxy (inosinate-cytidine) (50 ng  $\mu$ l $^{-1}$ )] at room temperature for 15 min. Protein-DNA complexes were separated using 5% (w/v) native PAGE and transferred to nylon membranes. Biotin-labeled probes were detected using the chemiluminescence detection instructions provided with the EMSA kit (Thermo Fisher Scientific; 20148). The sequence of the biotin-labeled probes was listed in data S6.

### ChIP followed by qPCR analysis (ChIP-qPCR)

ChIP assays were performed on WT, *FUL1*-OE, and *MYC2*-OE lines as described previously (58). The fruits were harvested when they reached the red ripening stage. They were then cross-linked with 1% (v/v) formaldehyde for 15 min under vacuum and quenched with 0.125 M glycine for 5 min under vacuum. After being washed three times, the samples were placed in liquid nitrogen for rapid freezing and then resuspended in ice-cold Honda buffer [0.44 M sucrose, 20 mM Hepes, 5 mM DTT, 1 mM phenylmethylsulfonyl fluoride (PMSF), 1.25% Ficoll 400, 2.5% Dextran 40, 0.5% Triton X-100, and

protease and phosphatase inhibitor] to isolate the nuclei. Filter samples through two layers of mira cloth (Millipore) at 4°C. The chromatin was precipitated and resuspended in nucleus dilution buffer [1 M tris-HCl (pH 8.0), 0.5 M EDTA, 10% SDS, 100 mM PMSF, and protease and phosphatase inhibitors]. The sample was then sonicated on the Bioruptor System for 15 min at 30% power, with 10-s on and 10-s off intervals, to shear DNA fragments ranging from 200 to 800 bp in length.

Chromatins were immunoprecipitated using protein A agarose beads and antibodies against FLAG (Cell Signaling Technologies; #14793) or H3K9ac (1/100, Cell Signaling Technologies; #9649 T), or H3K27ac (1/100, Cell Signaling Technologies; #8173). The mixture was then incubated overnight at 4°C. The beads underwent a series of washes, starting with a low salt buffer [0.1% (w/v) SDS, 1% (v/v) Triton X-100, 2 mM EDTA, 20 mM tris-HCl (pH 8.0), and 150 mM NaCl] followed by a high salt buffer [0.1% (w/v) SDS, 1% (v/v) Triton X-100, 2 mM EDTA, 20 mM tris-HCl (pH 8.0), and 500 mM NaCl], then a LiCl buffer [1% (w/v) sodium deoxycholate, 1% (v/v) NP-40, 1 mM EDTA, 10 mM tris-HCl (pH 8.0), and 250 mM LiCl], and lastly washes twice in TE buffer [1 mM EDTA and 10 mM tris-HCl (pH 8.0)]. The samples were incubated overnight at 65°C to reverse cross-linking. Afterward, they were incubated with Proteinase K (50 mg/ml, Cell Signaling Technologies; #10012S) at 65°C for 3 hours. The chromatin that was immunoprecipitated was dissolved in water for qPCR analysis.

## Y2H assay

The Y2H and β-galactosidase activity assays were conducted following the procedure of the Matchmaker Gold Y2H System (Clontech). The coding sequences for RIN and FUL1 were cloned into pGADT7 as prey constructs. Similarly, the coding sequences for RIN and FUL1 were also cloned into pGBKT7 to generate the bait constructs. In yeast strain AH109, different pairs of bait and prey constructs were cotransformed and grown on SD medium lacking Leu and Trp [double dropout supplements (DDO)] for 2 days. The yeast cultures were then incubated in SD medium lacking Leu, Trp, His, and Ade [quadruple detachment supplement (QDO)] and the QDO medium containing X-α-Gal (4 mg/ml; for blue color development). P53 and SV40 were used as positive control.

## Nuclei isolation and Western blotting

At the red stage, tomato fruits were harvested and their nuclei were isolated and assayed for FUL1-FLAG protein. The fruit samples were ground into a powder using liquid nitrogen and then extracted with a buffer containing 1 mM MgCl<sub>2</sub>, 10 mM tris-HCl (pH 7.5), 250 mM sucrose, 0.5% polyvinyl pyrrolidone, 0.5% Triton X-100, and Roche protease inhibitor tablets. The resulting suspension was filtered through mira cloth (Millipore). After centrifugation at 12,000 rpm for 15 min, the precipitate is washed with extraction buffer, centrifuged again at 12,000 rpm for 15 min, and then resuspended in Percoll buffer [10 mM tris-HCl (pH 7.5), 250 mM sucrose, 95% Percoll, and Roche protease inhibitor tablet]. After centrifugation at 12,000 rpm for 15 min, the floating layer was collected and then diluted to 30% with extraction buffer and centrifuged at 12,000 rpm for 15 min to precipitate the nuclei, which were ready for SDS-PAGE assay.

Western blotting was performed as described in ref. (55). Briefly, protein extracts were separated on 10% SDS-PAGE gels and then transferred to polyvinylidene difluoride (PVDF) membranes and

blocked with 5% skim milk for 2 hours at room temperature. The antibody against FLAG with horseradish peroxidase (HRP) (Cell Signaling Technologies; #14793) was added in a ratio of 1:1500 and incubated for 2 hours at room temperature. The membrane was washed three times with TBST buffer for 5 min each time. Last, the PVDF membranes were observed using an HRP-enhanced chemical staining system.

## Statistical analysis

All experiments were independently repeated at least three times, and results from representative datasets are presented. Statistical analysis was performed using Student's *t* test and one-way analysis of variance (ANOVA).

## Supplementary Materials

**The PDF file includes:**

Figs. S1 to S5

Legends for data S1 to S7

**Other Supplementary Material for this manuscript includes the following:**

Data S1 to S7

## REFERENCES AND NOTES

1. M. Itkin, U. Heinig, O. Tzfadia, A. J. Bhide, B. Shinde, P. D. Cardenas, S. E. Bocobza, T. Unger, S. Malitsky, R. Finkers, Y. Tikunov, A. Bovy, Y. Chikate, P. Singh, I. Rogachev, J. Beekwilder, A. P. Giri, A. Aharoni, Biosynthesis of antinutritional alkaloids in solanaceous crops is mediated by clustered genes. *Science* **341**, 175–179 (2013).
2. M. Itkin, I. Rogachev, N. Alkan, T. Rosenberg, S. Malitsky, L. Masini, S. Meir, Y. Iijima, K. Aoki, R. de Vos, D. Prusky, S. Burdman, J. Beekwilder, A. Aharoni, GLYCOALKALOID METABOLISM1 is required for steroidal alkaloid glycosylation and prevention of phytotoxicity in tomato. *Plant Cell* **23**, 4507–4525 (2011).
3. M. Friedman, Tomato glycoalkaloids: Role in the plant and in the diet. *J. Agric. Food Chem.* **50**, 5751–5780 (2002).
4. Y. Kazachkova, I. Zemach, S. Panda, S. Bocobza, A. Vainer, I. Rogachev, Y. Dong, S. Ben-Dor, D. Veres, C. Kanstrup, S. K. Lambertz, C. Crocoll, Y. Hu, E. Shani, S. Michaeli, H. H. Nour-Eldin, D. Zamir, A. Aharoni, The GORKY glycoalkaloid transporter is indispensable for preventing tomato bitterness. *Nat. Plants* **7**, 468–480 (2021).
5. M. Friedman, Potato glycoalkaloids and metabolites: Roles in the plant and in the diet. *J. Agric. Food Chem.* **54**, 8655–8681 (2006).
6. P. D. Sonawane, S. A. Gharat, A. Jozwiak, R. Barbole, S. Heinicke, E. Almekias-Siegli, S. Meir, I. Rogachev, S. E. O. Connor, A. P. Giri, A. Aharoni, A BAHD-type acyltransferase concludes the biosynthetic pathway of non-bitter glycoalkaloids in ripe tomato fruit. *Nat. Commun.* **14**, 4540 (2023).
7. D. K. Zhao, Y. Zhao, S. Y. Chen, E. J. Kennelly, Solanum steroidal glycoalkaloids: Structural diversity, biological activities, and biosynthesis. *Nat. Prod. Rep.* **38**, 1423–1444 (2021).
8. Y. You, J. A. L. van Kan, Bitter and sweet make tomato hard to (b)eat. *New Phytol.* **230**, 90–100 (2021).
9. P. D. Sonawane, A. Jozwiak, R. Barbole, S. Panda, B. Abebie, Y. Kazachkova, S. A. Gharat, O. Ramot, T. Unger, G. Wizler, S. Meir, I. Rogachev, A. Doron-Faigenboim, M. Petreikov, A. Schaffer, A. P. Giri, T. Scherf, A. Aharoni, 2-Oxoglutarate-dependent dioxygenases drive expansion of steroidal alkaloid structural diversity in the genus Solanum. *New Phytol.* **234**, 1394–1410 (2022).
10. J. Szymanski, S. Bocobza, S. Panda, P. Sonawane, P. D. Cardenas, J. Lashbrooke, A. Kamble, N. Shahaf, S. Meir, A. Bovy, J. Beekwilder, Y. Tikunov, I. Romero de la Fuente, D. Zamir, I. Rogachev, A. Aharoni, Analysis of wild tomato introgression lines elucidates the genetic basis of transcriptome and metabolome variation underlying fruit traits and pathogen response. *Nat. Genet.* **52**, 1111–1121 (2020).
11. P. D. Cárdenas, P. D. Sonawane, U. Heinig, A. Jozwiak, S. Panda, B. Abebie, Y. Kazachkova, M. Pliner, T. Unger, D. Wolf, I. Ofner, E. Vilaprinyo, S. Meir, O. Davydov, A. Gal-On, S. Burdman, A. Giri, D. Zamir, T. Scherf, J. Szymanski, I. Rogachev, A. Aharoni, Pathways to defense metabolites and evading fruit bitterness in genus Solanum evolved through 2-oxoglutarate-dependent dioxygenases. *Nat. Commun.* **10**, 5169 (2019).
12. Y. Liu, M. Du, L. Deng, J. Shen, M. Fang, Q. Chen, Y. Lu, Q. Wang, C. Li, Q. Zhai, MYC2 regulates the termination of jasmonate signaling via an autoregulatory negative feedback loop. *Plant Cell* **31**, 106–127 (2019).
13. P. D. Cardenas, P. D. Sonawane, J. Pollier, R. Vanden Bossche, V. Dewangan, E. Weithorn, L. Tal, S. Meir, I. Rogachev, S. Malitsky, A. P. Giri, A. Goossens, S. Burdman, A. Aharoni,

- GAME9 regulates the biosynthesis of steroidal alkaloids and upstream isoprenoids in the plant mevalonate pathway. *Nat. Commun.* **7**, 10654 (2016).
14. X. J. He, T. Chen, J.-K. Zhu, Regulation and function of DNA methylation in plants and animals. *Cell Res.* **21**, 442–465 (2011).
  15. J. A. Law, S. E. Jacobsen, Establishing, maintaining and modifying DNA methylation patterns in plants and animals. *Nat. Rev. Genet.* **11**, 204–220 (2010).
  16. H. Zhang, J. K. Zhu, Active DNA demethylation in plants and animals. *Cold Spring Harb. Symp. Quant. Biol.* **77**, 161–173 (2012).
  17. J. K. Zhu, Active DNA demethylation mediated by DNA glycosylases. *Annu. Rev. Genet.* **43**, 143–166 (2009).
  18. R. Liu, A. How-Kit, L. Stammitti, E. Teyssier, D. Rolin, A. Mortain-Bertrand, S. Halle, M. Liu, J. Kong, C. Wu, C. Degraeve-Guibault, N. H. Chapman, M. Maucourt, T. C. Hodgman, J. Tost, M. Bouzayen, Y. Hong, G. B. Seymour, J. J. Giovannoni, P. Galluscio, A DEMETER-like DNA demethylase governs tomato fruit ripening. *Proc. Natl. Acad. Sci. U.S.A.* **112**, 10804–10809 (2015).
  19. D. Cao, Z. Ju, C. Gao, X. Mei, D. Fu, H. Zhu, Y. Luo, B. Zhu, Genome-wide identification of cytosine-5 DNA methyltransferases and demethylases in *Solanum lycopersicum*. *Gene* **550**, 230–237 (2014).
  20. S. Zhong, Z. Fei, Y. R. Chen, Y. Zheng, M. Huang, J. Vrebalov, R. McQuinn, N. Gapper, B. Liu, J. Xiang, Y. Shao, J. J. Giovannoni, Single-base resolution methylomes of tomato fruit development reveal epigenome modifications associated with ripening. *Nat. Biotechnol.* **31**, 154–159 (2013).
  21. Z. Lang, Y. Wang, K. Tang, D. Tang, T. Datsenko, J. Cheng, Y. Zhang, A. K. Handa, J. K. Zhu, Critical roles of DNA demethylation in the activation of ripening-induced genes and inhibition of ripening-repressed genes in tomato fruit. *Proc. Natl. Acad. Sci. U.S.A.* **114**, E4511–E4519 (2017).
  22. S. Li, K. Chen, D. Grierson, A critical evaluation of the role of ethylene and MADS transcription factors in the network controlling fleshy fruit ripening. *New Phytol.* **221**, 1724–1741 (2019).
  23. M. Liu, J. Pirrello, C. Chervin, J. P. Roustan, M. Bouzayen, Ethylene control of fruit ripening: Revisiting the complex network of transcriptional regulation. *Plant Physiol.* **169**, 2380–2390 (2015).
  24. T. Chen, G. Qin, S. Tian, Regulatory network of fruit ripening: Current understanding and future challenges. *New Phytol.* **228**, 1219–1226 (2020).
  25. M. Bermer, R. Karlova, A. R. Ballester, Y. M. Tikhunov, A. G. Bovy, M. Wolters-Arts, B. Rossetto Pde, G. C. Angenent, R. A. de Maagd, The tomato FRUITFULL homologs TDR4/FUL1 and MBP7/FUL2 regulate ethylene-independent aspects of fruit ripening. *Plant Cell* **24**, 4437–4451 (2012).
  26. J. J. Giovannoni, Fruit ripening mutants yield insights into ripening control. *Curr. Opin. Plant Biol.* **10**, 283–289 (2007).
  27. K. Manning, M. Tör, M. Poole, Y. Hong, A. J. Thompson, G. J. King, J. J. Giovannoni, G. B. Seymour, A naturally occurring epigenetic mutation in a gene encoding an SBP-box transcription factor inhibits tomato fruit ripening. *Nat. Genet.* **38**, 948–952 (2006).
  28. J. Vrebalov, D. Ruezinsky, V. Padmanabhan, R. White, D. Medrano, R. Drake, W. Schuch, J. Giovannoni, A MADS-box gene necessary for fruit ripening at the tomato fruit ripening inhibitor (*rin*) locus. *Science* **296**, 343–346 (2002).
  29. Y. Iijima, Y. Fujiwara, T. Tokita, T. Ikeda, T. Nohara, K. Aoki, D. Shibata, Involvement of ethylene in the accumulation of esculenoside A during fruit ripening of tomato (*Solanum lycopersicum*). *J. Agric. Food Chem.* **57**, 3247–3252 (2009).
  30. Y. Gao, Y. Lin, M. Xu, H. Bian, C. Zhang, J. Wang, H. Wang, Y. Xu, Q. Niu, J. Zuo, D. Q. Fu, Y. Pan, K. Chen, H. Klee, Z. Lang, B. Zhang, The role and interaction between transcription factor NAC-NOR and DNA demethylase SIDM2 in the biosynthesis of tomato fruit flavor volatiles. *New Phytol.* **235**, 1913–1926 (2022).
  31. Z. Zhong, S. Feng, S. H. Duttkie, M. E. Potok, Y. Zhang, J. Gallego-Bartolome, W. Liu, S. E. Jacobsen, DNA methylation-linked chromatin accessibility affects genomic architecture in *Arabidopsis*. *Proc. Natl. Acad. Sci. U.S.A.* **118**, e2023347118 (2021).
  32. W. Huang, N. Hu, Z. Xiao, Y. Qiu, Y. Yang, J. Yang, X. Mao, Y. Wang, Z. Li, H. Guo, A molecular framework of ethylene-mediated fruit growth and ripening processes in tomato. *Plant Cell* **34**, 3280–3300 (2022).
  33. H. Deng, J. Pirrello, Y. Chen, N. Li, S. Zhu, X. Chirinos, M. Bouzayen, Y. Liu, M. Liu, A novel tomato F-box protein, SIEBF3, is involved in tuning ethylene signaling during plant development and climacteric fruit ripening. *Plant J.* **95**, 648–658 (2018).
  34. H. Jia, Y. Xu, Y. Deng, Y. Xie, Z. Gao, Z. Lang, Q. Niu, Key transcription factors regulate fruit ripening and metabolite accumulation in tomato. *Plant Physiol.* **195**, 2256–2273 (2024).
  35. R. Wang, E. Tavano, M. Lammers, A. P. Martinielli, G. C. Angenent, R. A. de Maagd, Re-evaluation of transcription factor function in tomato fruit development and ripening with CRISPR/Cas9-mutagenesis. *Sci. Rep.* **9**, 1696 (2019).
  36. M. Fujisawa, Y. Shima, H. Nakagawa, M. Kitagawa, J. Kimbara, T. Nakano, T. Kasumi, Y. Ito, Transcriptional regulation of fruit ripening by tomato FRUITFULL homologs and associated MADS box proteins. *Plant Cell* **26**, 89–101 (2014).
  37. S. Li, B. Zhu, J. Pirrello, C. Xu, B. Zhang, M. Bouzayen, K. Chen, D. Grierson, Roles of RIN and ethylene in tomato fruit ripening and ripening-associated traits. *New Phytol.* **226**, 460–475 (2020).
  38. F. Bai, P. Shu, H. Deng, Y. Wu, Y. Chen, M. Wu, T. Ma, Y. Zhang, J. Pirrello, Z. Li, Y. Hong, M. Bouzayen, M. Liu, A distal enhancer guides the negative selection of toxic glycoalkaloids during tomato domestication. *Nat. Commun.* **15**, 2894 (2024).
  39. M. Du, J. Zhao, D. T. W. Tzeng, Y. Liu, L. Deng, T. Yang, Q. Zhai, F. Wu, Z. Huang, M. Zhou, Q. Wang, Q. Chen, S. Zhong, C. B. Li, C. Li, MYC2 orchestrates a hierarchical transcriptional cascade that regulates jasmonate-mediated plant immunity in tomato. *Plant Cell* **29**, 1883–1906 (2017).
  40. Y. You, Q. Zhai, C. An, C. Li, LEUNIG\_HOMOLOG mediates MYC2-dependent transcriptional activation in cooperation with the coactivators HAC1 and MED25. *Plant Cell* **31**, 2187–2205 (2019).
  41. G. Zhu, S. Wang, Z. Huang, S. Zhang, Q. Liao, C. Zhang, T. Lin, M. Qin, M. Peng, C. Yang, X. Cao, X. Han, X. Wang, E. van der Knaap, Z. Zhang, X. Cui, H. Klee, A. R. Fernie, J. Luo, S. Huang, Rewiring of the fruit metabolome in tomato breeding. *Cell* **172**, 249–261.e12 (2018).
  42. Y. Zhou, Z. Zhang, Z. Bao, H. Li, Y. Lyu, Y. Zan, Y. Wu, L. Cheng, Y. Fang, K. Wu, J. Zhang, H. Lyu, T. Lin, Q. Gao, S. Saha, L. Mueller, Z. Fei, T. Stadler, S. Xu, Z. Zhang, D. Speed, S. Huang, Graph pangenome captures missing heritability and empowers tomato breeding. *Nature* **606**, 527–534 (2022).
  43. T. Lin, G. Zhu, J. Zhang, X. Xu, Q. Yu, Z. Zheng, Z. Zhang, Y. Lun, S. Li, X. Wang, Z. Huang, J. Li, C. Zhang, T. Wang, Y. Zhang, A. Wang, Y. Zhang, K. Lin, C. Li, G. Xiong, Y. Xue, A. Mazzucato, M. Causse, Z. Fei, J. J. Giovannoni, R. T. Chetelat, D. Zamir, T. Stadler, J. Li, Z. Ye, Y. Du, S. Huang, Genomic analyses provide insights into the history of tomato breeding. *Nat. Genet.* **46**, 1220–1226 (2014).
  44. E. V. Petersson, U. Arif, V. Schulzova, V. Krkova, J. Hajsova, J. Meijer, H. C. Andersson, L. Jonsson, F. Sitbon, Glycoalkaloid and calystegine levels in table potato cultivars subjected to wounding, light, and heat treatments. *J. Agric. Food Chem.* **61**, 5893–5902 (2013).
  45. H. Deng, Y. Chen, Z. Liu, Z. Liu, P. Shu, R. Wang, Y. Hao, D. Su, J. Pirrello, Y. Liu, Z. Li, D. Grierson, J. J. Giovannoni, M. Bouzayen, M. Liu, SIERF12 modulates the transition to ripening in tomato fruit by recruiting the co-repressor TOPLESS and histone deacetylases to repress key ripening genes. *Plant Cell* **34**, 1250–1272 (2022).
  46. G. Yu, C. Li, L. Zhang, G. Zhu, S. Munir, C. Shi, H. Zhang, G. Ai, S. Gao, Y. Zhang, C. Yang, J. Zhang, H. Li, Z. Ye, An allelic variant of GAME9 determines its binding capacity with the GAME17 promoter in the regulation of steroidal glycoalkaloid biosynthesis in tomato. *J. Exp. Bot.* **71**, 2527–2536 (2020).
  47. Y. Li, Y. Chen, L. Zhou, S. You, H. Deng, Y. Chen, S. Alseekh, Y. Yuan, R. Fu, Z. Zhang, D. Su, A. R. Fernie, M. Bouzayen, T. Ma, M. Liu, Y. Zhang, MicroTom metabolic network: Rewiring tomato metabolic regulatory network throughout the growth cycle. *Mol. Plant* **13**, 1203–1218 (2020).
  48. S. Chen, Y. Zhou, Y. Chen, J. Gu, fastp: An ultra-fast all-in-one FASTQ preprocessor. *Bioinformatics* **34**, i884–i890 (2018).
  49. H. Li, R. Durbin, Fast and accurate short read alignment with Burrows-Wheeler transform. *Bioinformatics* **25**, 1754–1760 (2009).
  50. B. Langmead, S. L. Salzberg, Fast gapped-read alignment with Bowtie 2. *Nat. Methods* **9**, 357–359 (2012).
  51. Y. Zhang, T. Liu, C. A. Meyer, J. Eeckhoute, D. S. Johnson, B. E. Bernstein, C. Nusbaum, R. M. Myers, M. Brown, W. Li, X. S. Liu, Model-based analysis of ChIP-Seq (MACS). *Genome Biol.* **9**, R137 (2008).
  52. L. Lopez-Delis, L. Rabbani, J. Wolff, V. Bhardwaj, R. Backofen, B. Gruning, F. Ramirez, T. Manke, pyGenomeTracks: Reproducible plots for multivariate genomic datasets. *Bioinformatics* **37**, 422–423 (2020).
  53. F. Ramirez, V. Bhardwaj, L. Arrigoni, K. C. Lam, B. A. Gruning, J. Villaveces, B. Habermann, A. Akhtar, T. Manke, High-resolution TADs reveal DNA sequences underlying genome organization in flies. *Nat. Commun.* **9**, 189 (2018).
  54. D. Kim, J. M. Paggi, C. Park, C. Bennett, S. L. Salzberg, Graph-based genome alignment and genotyping with HISAT2 and HISAT-genotype. *Nat. Biotechnol.* **37**, 907–915 (2019).
  55. M. Liu, Y. Chen, Y. Chen, J. H. Shin, I. Mila, C. Audran, M. Zouine, J. Pirrello, M. Bouzayen, The tomato Ethylene Response Factor SI-ERF.B3 integrates ethylene and auxin signaling via direct regulation of SI-Aux/IAA27. *New Phytol.* **219**, 631–640 (2018).
  56. S. Panda, A. Jozwiak, P. D. Sonawane, J. Szymanski, Y. Kazachkova, A. Vainer, H. Vasuki Kilambi, E. Almekias-Siegl, V. Dikaya, S. Bocobza, H. Shohat, S. Meir, G. Wizler, A. P. Giri, R. Schuurink, D. Weiss, H. Yasuor, A. Kamble, A. Aharoni, Steroidal alkaloids defence metabolism and plant growth are modulated by the joint action of gibberellin and jasmonate signaling. *New Phytol.* **233**, 1220–1237 (2022).
  57. S.-D. Yoo, Y.-H. Cho, J. Sheen, Arabidopsis mesophyll protoplasts: A versatile cell system for transient gene expression analysis. *Nat. Protoc.* **2**, 1565–1572 (2007).
  58. Y. Zhang, E. Butelli, S. Alseekh, T. Tohge, G. Rallapalli, J. Luo, P. G. Kawai, L. Hill, A. Santino, A. R. Fernie, C. Martin, Multi-level engineering facilitates the production of phenylpropanoid compounds in tomato. *Nat. Commun.* **6**, 8635 (2015).

**Acknowledgments:** We thank H. Wang from the Mass Spectrometry Core Facility in College of Life Sciences, Sichuan University for the assistance in metabolic analysis. We are grateful to

Z. Lang (Southern University of Science and Technology) and S. Li (Zhejiang University) for providing the *dml2* and *rin* mutants. **Funding:** This work was financially supported by grants from the National Natural Science Foundation of China to M.L. (nos. 31772780 and 32172643), the Applied Basic Research Category of Science and Technology Program of Sichuan Province to M.L. (2022YFSY0059-1 and 2021FYZ0010-5-LH), the Technology Innovation and Application Development Program of Chongqing to M.L. (cstc2021jscx-cyhX0001), the Institutional Research Funding of Sichuan University to M.L. (2022SCUNL105), the Guangxi Science and Technology Major Program to Y.W. (GuikeAA22068088), and the Fundamental research funds for the central universities to M.L. (SCU2024D003). **Author contributions:** F.B.: Writing—original draft, conceptualization, investigation, writing—review and editing, methodology, resources, data curation, validation, formal analysis, software, and visualization. M.W.: Data curation. W.H.: Resources and formal analysis. W.X.: Conceptualization, investigation, writing—review and editing, methodology, formal analysis, software, and visualization. Y.W.: Conceptualization, founding acquisition, and project administration. Y.Z.: Data curation. Z.Z.: Investigation and formal analysis. Y.H.: Writing—review and editing. J.P.: Writing—review and editing. M.B.: Conceptualization, writing—review and editing, methodology, validation, supervision, and

formal analysis. M.L.: Writing—original draft, conceptualization, writing—review and editing, resources, founding acquisition, data curation, validation, supervision, and project administration.

**Competing interests:** The authors declare that they have no competing interests. **Data and materials availability:** All data needed to evaluate the conclusions in the paper are present in the paper and/or the Supplementary Materials. The WGBS data of *dml2* and WT at 25- and 46-DPA from the NCBI database under GEO accession number GSE193170. The DNase-seq data and ChIP-seq data of NOR, RIN, MYC2, and histone from the NCBI database under BioProject accession numbers PRJNA309352, PRJNA381300, SRA046131, and PRJNA375842, respectively. The RNA-seq data of *dml2* from the NCBI database under GEO accession number GSE196474. The RNA-seq data of *nor*, *rin*, *ful1*, and *TF18* from the NCBI database under BioProject accession numbers PRJNA973565, GSE49289, and GSE49125, respectively.

Submitted 8 September 2024

Accepted 15 January 2025

Published 19 February 2025

10.1126/sciadv.ads9601